Thermobarometric constraints on the tectonothermal evolution of the East Humboldt Range metamorphic core complex, Nevada

Allen J. McGrew* *Department of Geology and Geophysics, University of Wyoming, Laramie, Wyoming 82071*

Mark T. Peters† *Department of Geophysical Sciences* and *Enrico Fermi Institute, University of Chicago, Chicago, Illinois 60637*

James E. Wright *Department of Geology and Geophysics, Rice University, Houston, Texas 77251*

ABSTRACT

The East Humboldt Range of Nevada provides a record of deep-crustal tectonic processes in a classic Cordilleran metamorphic core complex located in the hinterland of the Late Cretaceous to early Tertiary Sevier orogenic belt. New constraints reported here on the metamorphic history of this terrane suggest an overall clockwise pressure-temperature-time (*P-T-t*) path that began with deep tectonic burial and metamorphism at kyanite + staurolite + garnet grade before Late Cretaceous time (possibly in Late Jurassic time?). Subsequently, higher-temperature Late Cretaceous peak metamorphism overprinted this event, resulting in widespread partial melting and leucogranite injection contemporaneous with emplacement of a large-scale recumbent fold (the Winchell Lake nappe). A new $^{207}Pb^*/^{206}Pb^*$ date of 84.8 ± 2.8 Ma on syntectonic leucogranite from the hinge zone of this fold constrains the age of this major phase of tectonism. Metamorphism at this time probably reached the second sillimanite isograd, at least at deep structural levels, with peak *P-T* conditions of 800 °C and >9 kbar. High-grade conditions persisted during extensional tectonic denudation throughout much of Tertiary time. In conjunction with previously published work, the petrologic and thermobarometric results reported here for the northern East Humboldt Range delineate a steeply decompressional *P-T* trend that extends from ~9 kbar and 800 °C to 5 kbar and 630 °C. In the light of decompressional reaction textures, microstructural evidence, and previously published thermochronometric results, we interpret this trend as a *P-T-t* path for Late Cretaceous to Oligocene time. At least 2 kbar of this decompression (equivalent to at least 7 km of denudation) occurred in Late Cretaceous to early Tertiary time. This interpretation supports the idea that tectonic exhumation of deep-crustal rocks in northeastern Nevada began during or immediately after the closing stages of the Sevier orogeny. Finally, the steepness of the proposed *P-T-t* path implies a thermal evolution from a colder to a much hotter geotherm, a circumstance that probably requires plastic thinning of the lower plate in addition to brittle attenuation and removal of the upper plate during Tertiary extension.

INTRODUCTION

Delineating spatial and temporal variations in metamorphic conditions is essential to understanding the tectonic evolution of any crustal-scale orogenic system. Quantitative thermobarometry offers an important tool for constraining such relationships, especially when linked to detailed thermochronology and careful, field-based structural investigation. In this paper, we report thermobarometric results from the East Humboldt Range, Nevada, which represents the northern part of the Ruby Mountains–East Humboldt Range metamorphic core complex. As in other metamorphic core complexes in the western North American Cordillera, the East Humboldt Range presents a number of important tectonic problems that are best addressed through petrologic and thermobarometric investigation. Key questions include the following: (1) From what crustal levels did the East Humboldt Range originate? (2) What thermal conditions accompanied deformation, and what was the thermal structure and rheological condition of the crust during tectonism? (3) What pressure-temperature-time path (*P-T-t* path) did this terrane follow through its history, and how does this path constrain the timing, rate, and mechanism of tectonic processes such as burial, exhumation, and magmatic addition to the crust?

The disentanglement of the polyphase metamorphic history of the East Humboldt Range presents a formidable challenge that requires careful petrography and integration of available thermochronometric data.

This paper reports on one in a series of studies detailing the tectonothermal evolution of the East Humboldt Range. In other papers, McGrew and Snee (1994) have discussed $^{40}Ar/^{39}Ar$ thermochronometric results, and Peters and Wickham (1994) have discussed the metamorphic history as recorded by marble and calc-silicate units. The thermobarometric results reported here come primarily from deep-seated metapelites and, to a lesser extent, from metabasites in the northern and central part of the East Humboldt Range.

REGIONAL SETTING

The Ruby Mountains and East Humboldt Range lie in the northeastern part of the Basin and Range province in the hinterland of the Mesozoic Sevier fold-and-thrust belt and in the immediate foreland of the Antler orogenic belt (Fig. 1). Like many metamorphic core complexes, the Ruby–East Humboldt terrane records a complicated tectonic history, including at least two major orogenic events in Mesozoic time before tectonic exhumation during Tertiary extension. Oligocene tectonism has increasingly obscured older metamorphic and deformational events at the deepest structural levels in the Ruby–East Humboldt complex, but exposures at shallower structural levels docu-

*Present address: Department of Geology, University of Dayton, 300 College Park, Dayton, Ohio 45469-2364; e-mail: mcgrew@neelix.udayton.edu.

†Present address: Los Alamos National Laboratory, 1180 Town Center Drive, Las Vegas, Nevada 89134.

Data Repository item 20001 contains additional material related to this article.

GSA Bulletin; January 2000; v. 112; no. 1; p. 45–60; 5 figures; 3 tables.

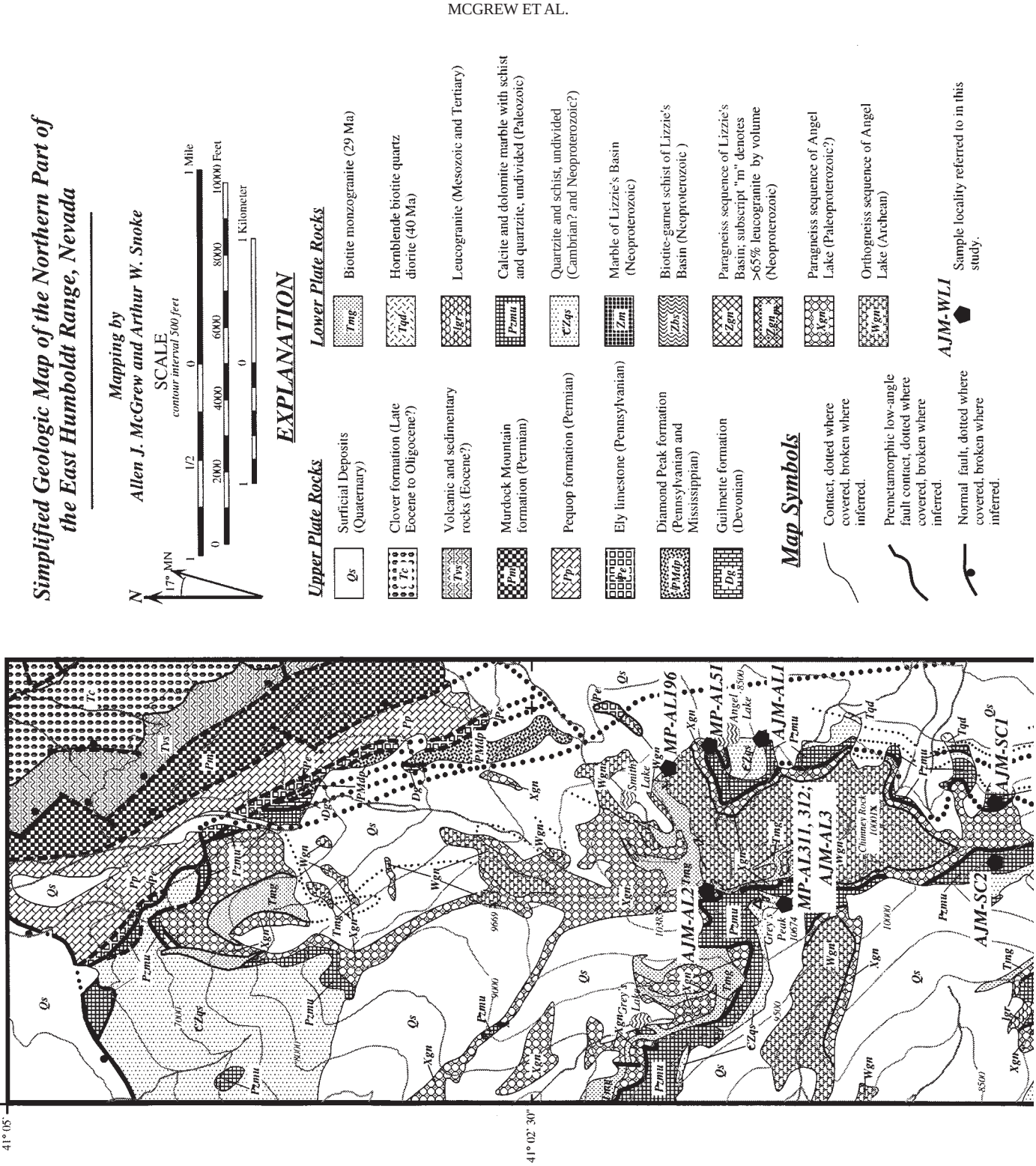

ment an intense and protracted pre-Oligocene tectonic history.

In the central Ruby Mountains, polyphase folding and upper-amphibolite-facies metamorphism occurred synkinematically with emplacement of Late Jurassic two-mica granite (Kistler et al., 1981; Hudec and Wright, 1990; Hudec, 1992). Farther north, Cretaceous and younger deformations largely obscure the Late Jurassic tectonic history. In the northern Ruby Mountains and the southern East Humboldt Range, U-Pb monazite ages on leucogranites and biotite schist document widespread Late Cretaceous migmatization, metamorphism, and large-scale deformation (Snoke et al., 1979; Snoke and Miller, 1988). In addition, $^{40}Ar/^{39}Ar$ muscovite and biotite cooling ages from the Wood Hills to the east suggest that peak metamorphism there was also Late Cretaceous in age and that final exhumation of the Wood Hills probably began by early Eocene time (Fig. 1)

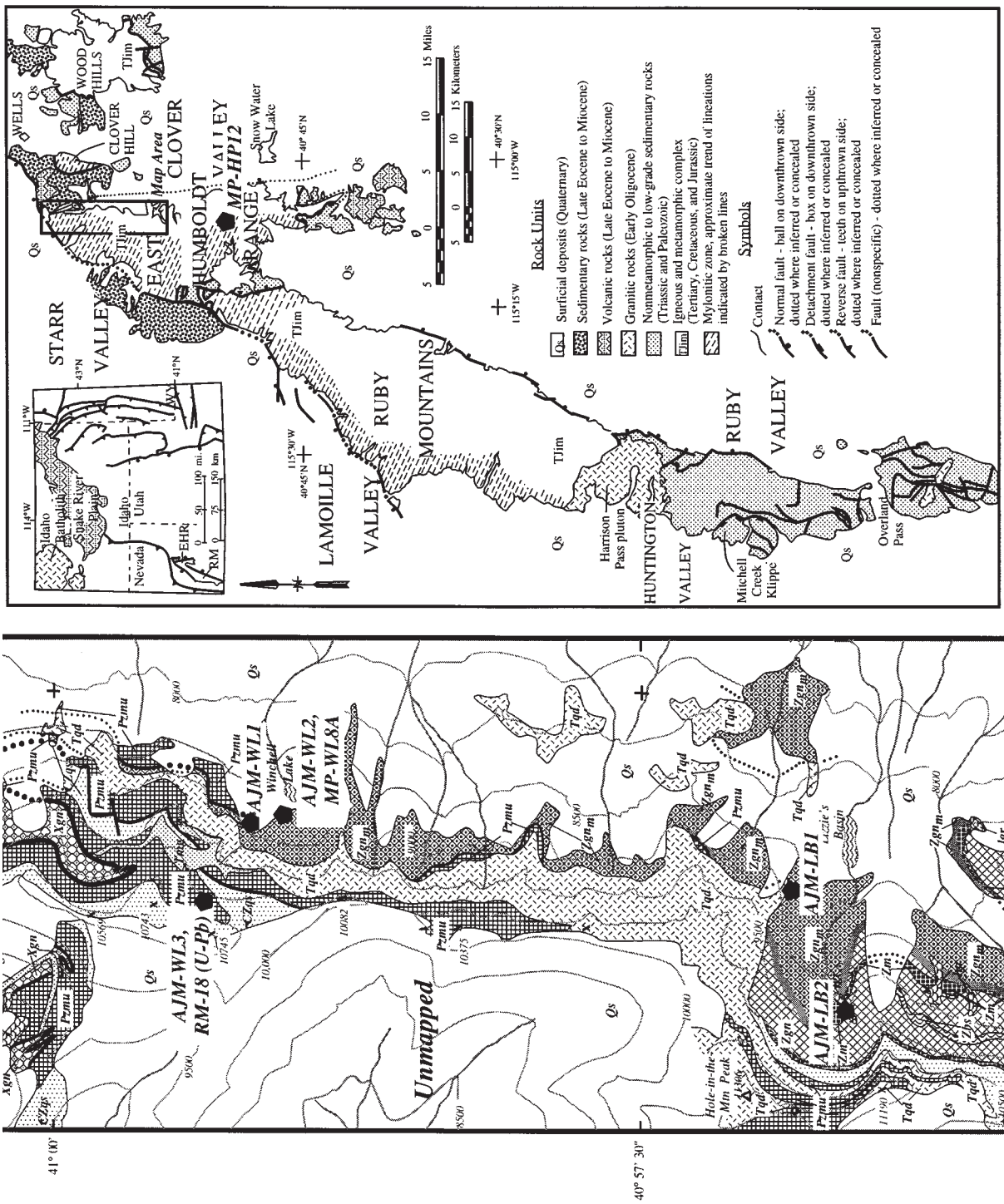

Figure 1. Geologic map of the northern part of the East Humboldt Range, Nevada, showing sample localities referred to in this study. Inset map shows the general geology of the Ruby–East Humboldt metamorphic core complex (after Snoke et al., 1990) and the regional tectonic setting of the study area relative to the Roberts Mountain allochthon to the west and the late Mesozoic Sevier orogenic belt to the east.

(Thorman and Snee, 1988; Camilleri and Chamberlin, 1997).

Overprinting and variably obscuring the older tectonic history is the gently west-dipping, >1-km-thick, normal-sense mylonitic shear zone that exhumed the Ruby Mountains and East Humboldt Range. This shear zone is well exposed along the western flank of the Ruby Mountains and East Humboldt Range for >150 km along strike, with the mylonites generally recording west-northwest–directed, normal-sense shear (Fig. 1) (Snoke and Lush, 1984; Snoke and Miller, 1988; Snoke et al., 1990; McGrew, 1992). Mylonitic fabrics overprint Tertiary granitoids ranging in age from 29 to 40 Ma, documenting an Oligocene or younger age for mylonitization (Wright and Snoke, 1993). $^{40}Ar/^{39}Ar$ hornblende and mica cooling ages and fission-track zircon, sphene, and apatite cooling ages record diachronous unroofing of the Ruby Mountains and East Humboldt Range from east-southeast to west-northwest be-

tween 35 and 20 Ma (Kistler et al., 1981; Dallmeyer et al., 1986; Dokka et al., 1986; McGrew and Snee, 1994).

The northern East Humboldt Range exposes a diverse suite of migmatitic upper-amphibolite-facies rocks arrayed as a stack of allochthons emplaced during the polyphase tectonic history (Fig. 1). One of these allochthons is a southward-closing recumbent isoclinal fold, the Winchell Lake nappe, that contains Archean orthogneiss and probable Paleoproterozoic paragneiss in its core (Snoke and Lush, 1984; Lush et al., 1988). Folded around this gneiss complex, and separated from it by an inferred prefolding, premetamorphic tectonic contact, is a metasedimentary sequence of quartzite, schist, and marble that we correlate to the Neoproterozoic to Mississippian (?) miogeoclinal sequence of the eastern Great Basin (McGrew, 1992). The marbles of this sequence repeat twice more in allochthons beneath the Winchell Lake nappe, with an allochthon of probable Neoproterozoic paragneiss intervening (Peters et al., 1992; Wickham and Peters, 1993). Inferred premetamorphic tectonic contacts bound each major package of rocks, and a thick sheet of hornblende-biotite quartz dioritic orthogneiss with a U-Pb zircon age of 40 ± 3 Ma cuts at low angle across the allochthons (Wright and Snoke, 1990). Abundant small bodies of biotite monzogranitic orthogneiss with an U-Pb zircon age of 29 Ma also cut across the various allochthons, but these intrusions are also partially involved in folding and extensively involved in mylonitic deformation (Wright and Snoke, 1986; McGrew and Snoke, 1990). The *P-T* results reported here come from metapelitic schists collected at various structural levels and from one metabasite collected from the Archean orthogneiss suite in the core of the Winchell Lake nappe above Angel Lake.

PREVIOUS WORK

Peters and Wickham (1994) investigated marble and calc-silicate petrogenesis in the study area and identified two distinct subassemblages. An early, diopside- and carbonate-rich assemblage probably equilibrated at ≥6 kbar, 550–750 °C, and relatively CO_2-rich fluid compositions, whereas a secondary subassemblage consisting of amphibole + epidote + garnet records infiltration by H_2O-rich fluids during metamorphism that proceeded from high-temperature (600–750 °C) to lower-temperature conditions (<525 °C) (Peters and Wickham, 1994). The timing of the older subassemblage relative to tectonic events is uncertain, but the secondary subassemblage grew during extensional exhumation, as seen from the fact that actinolitic amphibole locally grew in extensional microstructures such as normal-sense shear bands and veins oriented perpendicular to mylonitic stretching lineation (McGrew, 1992; Peters and Wickham, 1994).

In addition, previously published thermobarometric results exist for several surrounding areas, including the southwestern East Humboldt Range, the Ruby Mountains, the Wood Hills, and Clover Hill, a small terrane located between the northern East Humboldt Range and the Wood Hills (Fig. 1) (Kistler et al., 1981; Hudec, 1990; Hurlow et al., 1991; Hodges et al., 1992; Thorman and Snee, 1988; Camilleri and Chamberlin, 1997). Gibbs method and rim thermobarometric results from the northern Ruby Mountains and southwestern East Humboldt Range suggest that metamorphism there proceeded from 5.9–6.7 kbar and 675–775 °C during the Late Cretaceous to 3.1–4.2 kbar and 550–650 °C during Oligocene mylonitization (Hurlow et al., 1991; Hodges et al., 1992). $^{40}Ar/^{39}Ar$ hornblende data from the northern Ruby Mountains record cooling ages of 26 to 32 Ma, placing a lower bracket on the age of rim equilibration (Dallmeyer et al., 1986). $^{40}Ar/^{39}Ar$ hornblende data from the central and northern East Humboldt Range are more complicated but also indicate that rim equilibration could have occurred as late as the Tertiary (29–36 Ma at deep structural levels and 49–65 Ma at shallow structural levels) (McGrew and Snee, 1994). Additional evidence for high-grade metamorphism during Oligocene mylonitization includes the growth of high-temperature minerals in extensional microstructures such as shear bands and veins, dynamic recrystallization of feldspar porphyroclasts, and quartz crystallographic textures characteristic of upper-amphibolite-facies to granulite-facies conditions (McGrew, 1992; McGrew and Casey, 1998).

Gibbs method results from Clover Hill contrast with the previously described results, suggesting nearly isothermal decompression from pressures of 9–10 kbar to 5.0–6.4 kbar at 550–630 °C (Hodges et al., 1992). A single $^{40}Ar/^{39}Ar$ hornblende step-release spectrum from Clover Hill suggests partial degassing of hornblende following a thermal event before middle Cretaceous time (sample H16, Dallmeyer et al., 1986). On the basis of this age spectrum, Hodges et al. (1992) suggested that the isothermal decompression that they reported records an early episode of large-scale extensional unroofing in Late Jurassic or Early Cretaceous time. We note that this event is not recorded in the results reported here.

KEY FIELD RELATIONSHIPS AND AGE CONSTRAINTS

The East Humboldt Range exposes a diverse suite of metamorphic rocks representing a broad range of protolith types, including leucogranitic to dioritic orthogneiss, metabasite, calcite and dolomite marble, calc-silicate gneiss, metapelite, metapsammite, and metaquartzite. Within these lithologies there are few systematic spatial variations in mineral assemblage. A relict subassemblage including kyanite (and rarely also staurolite) occurs only on the upper limb of the Winchell Lake nappe. Muscovite is also much more abundant on the upper limb of the nappe, and assemblages including sillimanite and K-feldspar in the absence of muscovite occur locally at deep structural levels. In addition, isopleths of leucogranite abundance are mappable in some rock units, and these field relationships are critical for establishing relative timing constraints among the migmatitic, metamorphic, and tectonic events.

The most systematic increase in leucogranite abundance occurs at the deepest structural levels in the East Humboldt Range, beneath the hornblende-biotite quartz diorite sill in the paragneiss sequence of Lizzie's Basin (Fig. 1). Here, the visually estimated volume proportion of leucosome and small granitic bodies increases systematically from values of generally <50% above 2865 m (9400 ft) to values of >65% (locally >90%) at elevations below 2745 m (9000 ft) (McGrew, 1992; Peters and Wickham, 1995). Textural relationships, such as fine-scale interdigitations of leucosome and melanosome, suggest that some rocks represent in situ partial melts, but the sheer volume of leucogranite suggests that a sizable fraction must emanate from deeper structural levels (Peters and Wickham, 1995). We informally name this sequence of extremely migmatitic rocks "the migmatite complex of Lizzie's Basin" and define the 65% leucogranite isopleth as its upper boundary, although we note that this transition is actually gradational across a narrow interval. Map-scale, fingerlike bodies of leucogranite originating from the Lizzie's Basin migmatite complex locally protrude upward into the overlying rocks (Fig. 1). No ages currently exist for the Lizzie's Basin leucogranite suite, and more than one generation of leucogranite is probably present. However, some leucogranitic bodies cut the 40 Ma quartz dioritic sill and the 29 Ma monzogranitic sheets.

The roof of the migmatite complex of Lizzie's Basin also coincides with an important oxygen isotope discontinuity and with the nearly complete replacement of marble by calc-silicate gneiss below (Wickham and Peters, 1990; Wickham et al., 1991; McGrew, 1992; Peters and Wickham, 1995). The metasedimentary rocks of the migmatite complex exhibit uniformly low $\delta^{18}O$ values implying equilibration with a large, isotopically light fluid reservoir, whereas rocks at higher elevations show higher and generally more variable $\delta^{18}O$ values (Wickham and Peters, 1990; Peters and Wickham, 1995). Furthermore, all calc-silicate samples in the Lizzie's Basin migmatite complex show extensive overgrowths of amphibole ±

epidote ± garnet, suggesting a late-stage, high-temperature, H_2O-rich fluid infiltration event (Peters and Wickham, 1994). In addition, where this late-stage assemblage is well developed at shallower structural levels, it is generally associated with nearby leucogranites, further documenting the tie between metamorphism and magmatism (Peters and Wickham, 1994, 1995). Therefore, we infer that fluids and heat derived from these melts were important factors in metamorphism. Finally, the late-stage assemblage occurs locally in extensional shear bands, pull-apart zones, or veins orthogonal to stretching lineation, suggesting a synextensional origin for both the migmatite complex of Lizzie's Basin and the final episode of H_2O-rich high-grade metamorphism.

Variations in the amount of leucogranite above the migmatite complex of Lizzie's Basin are more localized and related to host lithology: marbles and pure quartzites generally contain <10% leucogranite, whereas pelitic or semipelitic units and quartzofeldspathic gneiss contain variable amounts of leucogranite, ranging from <15% to >75% by volume (McGrew, 1992).

Migmatitic relationships in one particular unit on the upper limb of the Winchell Lake nappe are crucial for constraining the age of migmatization, sillimanite-grade metamorphism, and nappe emplacement. The unit of interest is a distinctive rusty-weathering, graphite-rich pelitic to semipelitic schist that shows a profound variation in volume percent leucogranite from <25% to >65% over a distance of ~2 km as it is traced from the upper limb into the hinge zone of the Winchell Lake nappe (Fig. 1) (McGrew, 1992). This unit can be mapped continuously over this distance and shows a relatively constant thickness of ~25 m. Commonly, the leucogranite occurs as small pods and seams intricately interlayered with selvages enriched in biotite, iron oxide, and graphite, suggesting that much of this leucosome originated by in situ partial melting. In addition, the relative paucity of leucogranite in surrounding marbles suggests that these small leucogranite bodies were mostly internally and not externally derived.

On the lower limb of the nappe, the rusty-weathering graphitic schist unit never exceeds 5 m in thickness, and in most localities it is completely absent or exists only as isolated rafts of graphitic, biotite-rich melanosome suspended in small bodies of leucogranite a few meters in size. We suggest that a higher percentage of melting (possibly driven by a flux of water) on the lower limb of the nappe combined with tectonic kneading to expel much of the melt, entraining rafts of melanosome as well. A difference in the degree of partial melting and the associated tectonic response would explain why the graphitic schist horizon, which is so conspicuous and continuous on the upper limb of the nappe, is nearly but not completely absent on the lower limb. This interpretation implies a synkinematic relationship between migmatization and nappe emplacement. Supporting this interpretation is the fact that migmatitic layering in this unit folds around the hinge line of the nappe (i.e., the layering is prekinematic to synkinematic), whereas isopleths of leucogranite abundance cut the nappe (i.e., they are synkinematic to postkinematic). Taken together, these relationships imply that melting must have been synkinematic with nappe emplacement.

Finally, we argue that the relationships also constrain the age of an important phase of sillimanite-grade metamorphism in the East Humboldt Range. Kyanite occurs only on the upper limb of the nappe, where it is usually severely resorbed and thickly mantled by fibrous sprays of sillimanite. It occurs most commonly in relatively nonmigmatitic parts of the rusty-weathering graphitic schist unit, and its disappearance coincides with the increasing abundance of leucogranite in this unit, suggesting that the replacement of kyanite by sillimanite was facilitated by the same processes that produced the leucogranites in this unit. Consistent with this interpretation, crenulation cleavage oriented parallel to the axial surface of the Winchell Lake nappe commonly folds dense mats or sprays of sillimanite, indicating that a major phase of sillimanite growth must have been prekinematic or early synkinematic to folding. In addition, sillimanite typically parallels compositional layering even where compositional layering is steeply inclined in the hinge zones of major folds, including the Winchell Lake nappe itself. Consequently, the older, kyanite-grade metamorphism must have occurred before nappe emplacement. We suggest that kyanite-grade metamorphism in the East Humboldt Range may have been synchronous with kyanite growth in Clover Hill (i.e., Early Cretaceous or older) (Hodges et al., 1992).

GEOCHRONOLOGICAL DATA AND INTERPRETATION

In light of the described relationships, the timing of both nappe emplacement and metamorphism hinges on the age of migmatization in the rusty-weathering graphitic schist horizon. Here we report new age data based on three zircon fractions from a meter-scale body of leucogranite collected from the graphitic schist unit in the hinge zone of the Winchell Lake nappe within a few meters of thermobarometry sample locality AJM-WL3 (Fig. 1, Table 1). All fractions were heavily abraded and carefully handpicked in order to avoid crystals with cores of premagmatic zircon. Apparently, we succeeded in avoiding older, premagmatic zircon components because all $^{207}Pb^*/^{206}Pb^*$ dates are indistinguishable within analytical error (Table 1). Because of the limited spread in U-Pb dates and the complete agreement of the $^{207}Pb^*/^{206}Pb^*$ dates from each of the analyzed fractions, we interpret the age of this sample to be the weighted mean of the $^{207}Pb^*/^{206}Pb^*$ dates, 84.8 ± 2.8 Ma (mean square of weighted deviates [MSWD] = 3).

The body of leucogranite from which this sample originated was actually folded around the nose of the Winchell Lake nappe at this locality, and so at a minimum this date represents an older age limit for nappe emplacement. However, because the isopleths of leucogranite abundance in the graphitic schist unit cut the nappe, this age also must represent a *younger* age limit for nappe emplacement. Taken together, these relationships imply that leucogranite generation could only have been synchronous with nappe emplacement, as already described. Secondary constraints on the age of nappe emplacement are provided by the observations that the 40 Ma quartz diorite sill cuts the base of the nappe and some of the 29 Ma biotite monzogranitic bodies also cut the nappe at map scale (Fig. 1). However, the nappe was certainly strongly modified and perhaps even amplified after Late Cretaceous time because many of the 29 Ma biotite monzogranitic bodies are partially to wholly involved in outcrop-scale folds. Such a polyphase tectonic history is not at all surprising because the entire Winchell Lake nappe is engulfed by the well-dated Tertiary mylonitic zone, and the nappe's hinge line has been transposed into parallelism with the mylonitic stretching lineation.

PETROGRAPHY, PHASE RELATIONSHIPS, AND MINERAL CHEMISTRY

One metabasite and 19 metapelite samples from a range of structural levels both within and beneath the mylonitic shear zone were chosen for detailed microanalysis and thermobarometric investigation (Fig. 1; Table 2). Four of the metapelitic samples yielded poorly constrained results that we discuss no further here, but the GSA Data Repository[1] includes a detailed summary of the mineral chemistry, mineral-zoning profiles, average electron-microprobe analyses, and *P-T* results for each sample investigated. In addition to optical examination, minerals in each sample were analyzed on the Cameca MBX microprobe at the University of Wyoming, the Cameca SX-50 microprobe at Purdue University, or the Cameca SX-50 microprobe at the University of Chicago. WDS (wavelength-dispersive spectroscopy) operating conditions included an accelerating volt-

TABLE 1. U-Pb ISOTOPIC DATA

Sample[†]	U (ppm)	$^{206}Pb^*$ (ppm)	Measured ratios[§]			Atomic ratios			Apparent ages[#] (Ma)		
			$\frac{^{206}Pb}{^{204}Pb}$	$\frac{^{207}Pb}{^{206}Pb}$	$\frac{^{208}Pb}{^{206}Pb}$	$\frac{^{206}Pb^*}{^{238}U}$	$\frac{^{207}Pb^*}{^{235}U}$	$\frac{^{207}Pb^*}{^{206}Pb^*}$	$\frac{^{206}Pb^*}{^{238}U}$	$\frac{^{207}Pb^*}{^{235}U}$	$\frac{^{207}Pb^*}{^{206}Pb^*}$
RM-18A	2176	21.46	74237	0.04789	0.00717	0.01148(6)	0.07549(38)	0.04770(3)	73.6	73.9	84.2 ± 1.6
RM-18B	2144	21.08	87148	0.04786	0.00694	0.01145(6)	0.07529(38)	0.04769(2)	73.4	73.7	84.0 ± 1.1
RM-18C	2288	23.21	12686	0.04889	0.01022	0.01180(6)	0.07769(39)	0.04773(3)	75.7	76.0	86.1 ± 1.4

Notes: Sample dissolution and ion exchange chemistry modified from Krogh (1973). U and Pb concentrations determined by isotope dilution via the addition of a mixed ^{208}Pb-^{235}U tracer added to solution aliquots of each sample. Pb blanks have varied from 10 to 30 pg.

*Radiogenic Pb, corrected for common Pb using the isotopic composition of $^{206}Pb/^{204}Pb = 18.6$ and $^{207}Pb/^{204}Pb = 15.6$.

[†]Sample masses were all ~0.1 mg; all fractions were heavily abraded.

[§]Isotopic compositions corrected for mass fractionation (0.11% per atomic mass unit).

[#]Ages calculated using the following constants: decay constants for ^{235}U and $^{238}U = 9.8485 \times 10^{-10}$ and 1.55125×10^{-10} yr^{-1}, respectively; $^{238}U/^{235}U = 137.88$. Error analysis follows Mattinson (1987).

age of 15 keV, a beam current of 20, 25, or 30 nA, and a spot size of 10 μm in order to avoid problems due to surface roughness. Natural and synthetic minerals were used as standards.

In each sample, we identified two or three domains in which the minerals relevant to key equilibria occurred in mutual contact. In each domain, rim compositions were analyzed, and average rim compositions based on two to eight analyses were calculated. Rarely, a given mineral was so sparse that only a single grain could be analyzed. To check for zoning, we analyzed both cores and rims of variable-composition phases such as garnet, plagioclase, biotite, amphibole, pyroxene, and staurolite. In addition, we constructed detailed zoning profiles for garnet and occasionally for other minerals.

Metabasites

Amphibolites occur most commonly in the Paleoproterozoic and Archean gneiss sequences of Angel Lake near the northern end of the range, where they probably represent metamorphosed small mafic intrusions. However, small bodies of amphibolite also occur locally in the paragneiss sequence of Lizzie's Basin, and rarely in the inferred Paleozoic metasedimentary sequence, where field relationships with adjacent calc-silicate layers typically suggest a sedimentary rather than an igneous origin. In order of decreasing abundance, metabasite mineral assemblages commonly include amphibole + plagioclase ± biotite ± garnet ± quartz ± clinopyroxene ± ilmenite ± sphene ± magnetite ± rutile ± apatite ± chlorite ± calcite ± white mica. Table 2 gives the observed mineral assemblage and locality information for sample MP-AL196, which is discussed in detail here. A detailed summary of the mineral chemistry is provided in the GSA Data Repository (see text footnote 1).

Of the minerals listed, calcite and white mica are quite sparse, occurring locally in fine veins or as secondary alteration of plagioclase. Chlorite is also secondary and occurs most commonly along normal-sense shear bands, in veins oriented at high angle to foliation, or in pull-apart zones in hornblende, biotite, or garnet. Locally, biotite also fills veins, but it occurs most abundantly as a replacement for hornblende at deep structural levels. In some localities in the Lizzie's Basin migmatite complex, biotite nearly completely replaces centimeter-scale to meter-scale boudins of amphibolite, with only the cores of the boudins preserving amphibole-rich assemblages. Such relationships require metasomatic introduction of potassium and H_2O, consistent with relationships in the nearby calc-silicate lithologies. As in the calc-silicate assemblages, the necessary fluid fluxes to drive such metasomatic replacements probably came from the crystallization of the surrounding leucogranites (Peters and Wickham, 1994).

Many amphibolites contain moderately to severely resorbed garnet porphyroblasts ranging from 1 mm to as much as 2 cm in size. A symplectite of plagioclase ± hornblende ± biotite commonly mantles or completely replaces such garnets (Fig. 2A). Sample MP-AL196 contains 0.5–1 mm subhedral garnets rimmed by a symplectite of amphibole + plagioclase. This is probably a decompression texture based on a reaction such as

$$\text{amphibole1} + \text{plagioclase} = \text{garnet} + \text{quartz} + \text{amphibole2}, \quad (1)$$

where amphibole1 coexisting with plagioclase in the symplectite is less sodic and less aluminous than amphibole2 in the matrix (Kohn and Spear, 1989, 1990). Because of its small dP/dT, this reaction is a useful geobarometer, and the observed texture implies a decompressional P-T path.

Consistent with this interpretation, the garnets in MP-AL196 show minor zoning near the rims characterized by depletion in Ca and enrichment in Fe, Mg, and Mn where the garnet is in contact with the symplectite texture. Plagioclase in the symplectite is calcic (An_{80}–An_{90}) and resembles the rims of matrix grains (An_{80}–An_{85}), whereas the core compositions of matrix grains are typically less calcic (An_{50}–An_{55}). Some grains are unzoned, but reverse zoning is common, consistent with the growth of calcic plagioclase at the expense of garnet. The amphibole is mostly edenitic hornblende (Leake, 1978) and plots in the low-pressure facies series (= the sillimanite-zone field) of Laird and Albee (1981). It shows slight decreases in Al/Si toward the rim, consistent with decreasing temperature during metamorphism (Laird and Albee, 1981). Symplectic hornblende is uniform in composition and resembles the rims of matrix grains, but it is typically less sodic and less aluminous than matrix cores, consistent with reaction 1.

Coexisting with the edenitic hornblende are less abundant discrete grains of actinolite (Leake, 1978). Given the occurrence of actinolite as discrete grains adjacent to hornblende, and not as exsolution lamellae, the coexistence of these two phases probably does not represent an immiscibility phenomenon. Rather, the actinolite probably formed as a late-stage product of a retrograde reaction such as

$$\text{hornblende} + \text{quartz} = \text{actinolite} + \text{albite}. \quad (2)$$

Cooper (1972) proposed this as an important reaction in metabasites at temperatures of the garnet isograd. Supporting this interpretation, plagioclase adjacent to actinolite and hornblende typically shows more albite-rich rims than observed elsewhere in the sample.

Although ilmenite is not present in sample MP-AL196, in many metabasites, ilmenite and plagioclase form a symplectite replacing sphene (Fig. 2B). This is probably a decompression texture based on a reaction such as

$$3\ \text{almandine} + 5\ \text{tschermakite} + 9\ \text{sphene}$$

[1]GSA Data Repository item 20001, data tables and zoning profile figures, is available on the Web at http://www.geosociety.org/pubs/drpint.htm. Requests may also be sent to Documents Secretary, GSA, P.O. Box 9140, Boulder, CO 80301; e-mail: editing@geosociety.org.

TABLE 2. MINERAL ASSEMBLAGES AND SAMPLE LOCALITY INFORMATION

Sample*	Latitude (north)	Longitude (west)	Elevation	Assemblage†
Metapelites				
AJM-AL1	41°01′25″	115°05′13″	2633 m (8640 ft)	bt+sil+gt+q+ksp+pl+mu
AJM-AL2	41°01′25″	115°05′13″	3121 m (10240 ft)	bt+sil+gt+q+ru+ilm+(chl)
MP-AL311	41°01′21″	115°06′12″	3194 m (10480 ft)	gt+bt+sil +pl+q+ilm+ru
MP-AL312	41°01′20″	115°06′13″	3197 m (10490 ft)	gt+bt+mu+sil+pl+q+ilm+ru+st
AJM-AL3	41°01′19″	115°06′13″	3194 m (10480 ft)	bt+sil+gt+q+pl+mu+ru+(chl)
MP-AL51	41°01′37″	115°05′15″	2566 m (8420 ft)	gt+bt+sil+pl+q+ilm+ru±ksp+(chl)
AJM-SC1	41°00′17″	115°05′36″	2798 m (9180 ft)	bt+sil+gt+q+pl+ru+ilm
AJM-SC2	41°00′17″	115°05′57″	3078 m (10100 ft)	bt+sil+[ky]+gt+q+pl+ru+ilm
AJM-WL1	40°59′08″	115°05′46″	2731 m (8960 ft)	bt+sil+gt+q+ksp+pl+ru
AJM-WL2	40°59′01″	115°05′45″	2670 m (8760 ft)	bt+gt+[st]+cd+sp+pl+[oa]+[ru]+ilm+cor+(sil)+(chl)
MP-WL8A	40°59′01″	115°05′45″	2670 m (8760 ft)	gt+bt+sil+pl+q+ilm+ru+cd+(chl)
AJM-WL3	40°59′20″	115°06′13″	3133 m (10280 ft)	bt+sil+gt+q+pl+ru+ilm
AJM-LB1	40°56′50″	115°06′21″	2640 m (8660 ft)	bt+sil+gt+q+ksp+pl+ru
AJM-LB2	40°56′38″	115°06′48″	2731 m (8960 ft)	bt+sil+gt+q+pl+ilm+(chl)
MP-LB132	40°55′54″	115°07′27″	3200 m (10500 ft)	gt+bt+mu+sil+q+ilm+ru
MP-LB134	40°56′55″	115°06′35″	2860 m (9380 ft)	gt+bt+sil+pl+q+ilm+ru
MP-LB135	40°56′55″	115°06′35″	2860 m (9380 ft)	gt+bt+sil+pl+q+ilm+ru
MP-HP12	40°50′59″	115°05′12″	2588 m (8490 ft)	gt+bt+mu+sil+pl+q
Metabasite				
MP-AL196	41°01′52″	115°05′20″	2780 m (9120 ft)	[gt]+amph+cpx+pl+q+sph+ru

*Sample name abbreviations: AJM—sample collected by McGrew, MP—sample collected by Peters, AL—Angel Lake cirque, HP—Humboldt Peak, LB—Lizzie's Basin, SC—Schoer Creek, WL—Winchell Lake cirque.

†Texturally early minerals in square brackets; texturally late minerals in parentheses. Mineral abbreviations: amph—amphibole, bt—biotite, chl—chlorite, cd—cordierite, cor—corundum, cpx—clinopyroxene, gt—garnet, ilm—ilmenite, ksp- K-feldspar, ky—kyanite, oa—orthoamphibole, pl—plagioclase, q—quartz, ru—rutile, sil—sillimanite, sph—sphene, sp—spinel, st—staurolite.

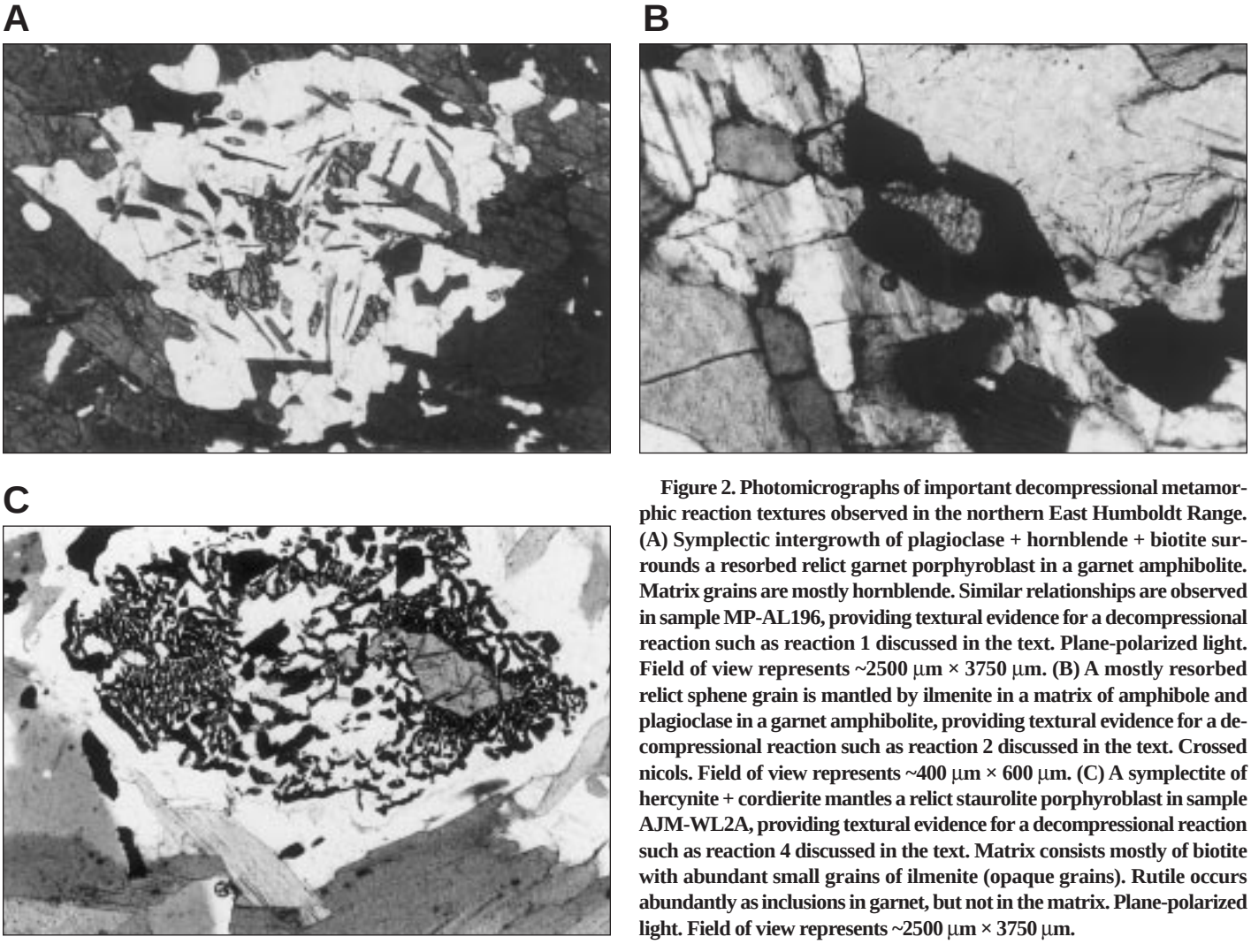

Figure 2. Photomicrographs of important decompressional metamorphic reaction textures observed in the northern East Humboldt Range. (A) Symplectic intergrowth of plagioclase + hornblende + biotite surrounds a resorbed relict garnet porphyroblast in a garnet amphibolite. Matrix grains are mostly hornblende. Similar relationships are observed in sample MP-AL196, providing textural evidence for a decompressional reaction such as reaction 1 discussed in the text. Plane-polarized light. Field of view represents ~2500 μm × 3750 μm. (B) A mostly resorbed relict sphene grain is mantled by ilmenite in a matrix of amphibole and plagioclase in a garnet amphibolite, providing textural evidence for a decompressional reaction such as reaction 2 discussed in the text. Crossed nicols. Field of view represents ~400 μm × 600 μm. (C) A symplectite of hercynite + cordierite mantles a relict staurolite porphyroblast in sample AJM-WL2A, providing textural evidence for a decompressional reaction such as reaction 4 discussed in the text. Matrix consists mostly of biotite with abundant small grains of ilmenite (opaque grains). Rutile occurs abundantly as inclusions in garnet, but not in the matrix. Plane-polarized light. Field of view represents ~2500 μm × 3750 μm.

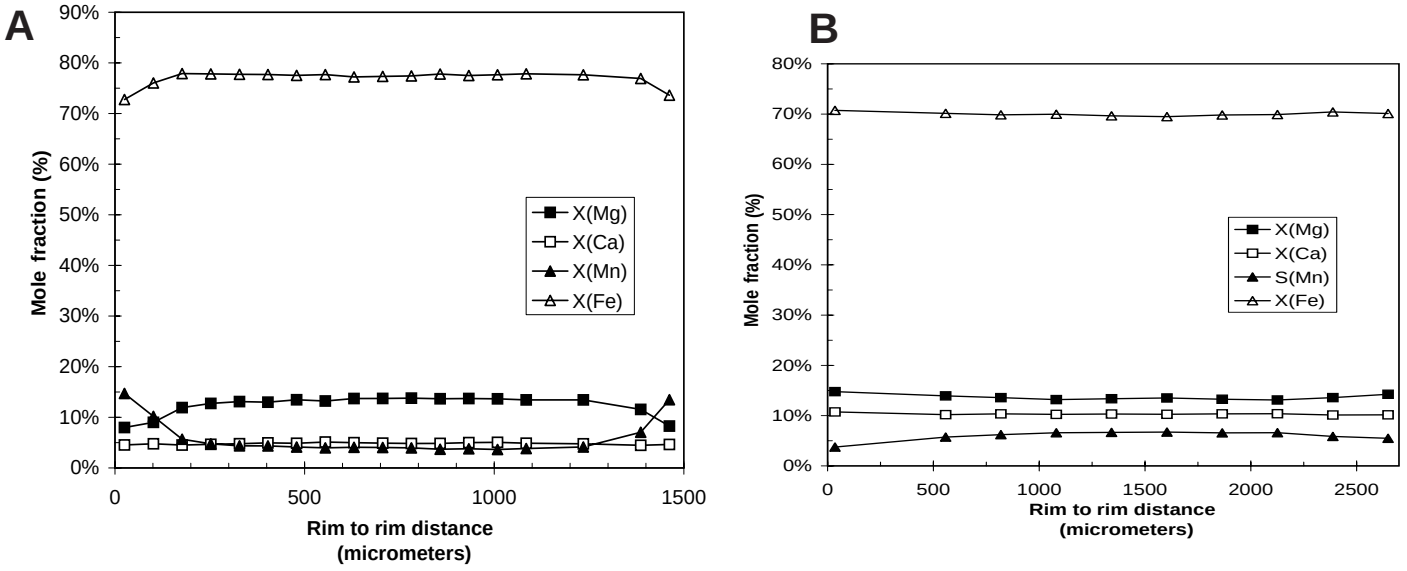

Figure 3. Examples of garnet zoning profiles. (A) Garnet zoning profile for sample AJM-AL3 exemplifying the most common profile type observed in the East Humboldt Range. (B) Garnet zoning profile for sample AJM-SC1 showing a less common, bell-shaped X_{Mn} profile developed in an unusually idioblastic garnet porphyroblast.

$$+ 2 \text{ quartz} = 13 \text{ anorthite} + 3 \text{ tremolite} + 9 \text{ ilmenite} + 2\ H_2O. \quad (3)$$

This reaction has a relatively shallow slope in *P-T* space with sphene and garnet on the high-pressure side of the reaction (dP/dT = 0.016 kbar/°C according to Thermocalc) (Powell and Holland, 1988). Consequently, this reaction implies a decompressional *P-T* trajectory compatible with rapid unroofing during the course of metamorphism, reinforcing the interpretation of reaction 1.

Metapelitic Rocks

Table 2 summarizes mineral assemblages in the metapelitic rocks and provides information on sample localities (see also Fig. 1). Except for samples AJM-WL2A and AJM-WL2B (discussed separately later), the characteristic assemblage consists of biotite + sillimanite + garnet + quartz + plagioclase ± chlorite ± muscovite ± K-feldspar ± rutile ± ilmenite. In addition, we noted the occurrence of kyanite and/or staurolite as relict phases in a few localities on the upper limb of the Winchell Lake nappe, where they form inclusions in garnet or, in the case of kyanite, matrix porphyroblasts thickly mantled by sillimanite (samples AJM-SC2 and MP-AL312). These rare occurrences of kyanite and staurolite record the oldest metamorphism observed in the East Humboldt Range and must be prekinematic relative to the Winchell Lake nappe (see Key Field Relationships and Age Constraints). They define a subassemblage similar to peak-metamorphic assemblages in the Wood Hills, where *P-T* conditions in the range 540–590 °C and 5.5–6.5 kbar probably occurred before 115 Ma (Hodges et al., 1992).

Garnet is the only mineral to show appreciable zoning. The cores of a few of the largest porphyroblasts (≥1 cm diameter) show relatively complicated zoning, but most show broad, relatively homogeneous cores with increasing spessartine component and decreasing pyrope component near the rim (Fig. 3A). Zoning profiles of this type are common in high-grade rocks and resemble garnet profiles previously reported from the Ruby Mountains and East Humboldt Range (Hurlow et al., 1991; Hodges et al., 1992). Concentration of manganese in the rims probably reflects resorption and partial replacement of high-grade garnet by minerals such as biotite and chlorite (Tracy, 1982). Consequently, *P-T* results reported here based on garnet-rim compositions probably record post–peak metamorphism. Garnet zoning profiles in samples AJM-SC1 and AJM-SC2 differ slightly from those already described, showing slight decreases in spessartine component and increases in pyrope and grossular component toward the rim, with almandine nearly constant (Fig. 3B). Bell-shaped X_{Mn} profiles of this type probably reflect preferential fractionation of manganese into garnet relative to other minerals during garnet growth (Hollister, 1966; Tracy, 1982). These garnets are idioblastic with little evidence of resorption at grain boundaries, compatible with this interpretation.

As previously noted, much of the sillimanite is involved in microfolding and must be prekinematic or synkinematic to the Winchell Lake nappe formation. In addition, bundles of fibrolite and prismatic grains of sillimanite are locally boudinaged, cut by extensional crenulation cleavage, or cut by microfractures oriented perpendicular to Tertiary stretching lineation. Nevertheless, many metapelites show multiple phases of sillimanite growth, and the final phase probably occurred during Oligocene extension. For example, extensional shear bands characterized by intense grain-size reduction locally show very fine fibrolite intergrown with dynamically recrystallized quartz and fine-grained biotite, implying growth synkinematic to the early stages of mylonitic deformation. In addition, very fine fibrolite locally fills pull-apart zones in microboudinaged prisms of sillimanite, indicating that sillimanite continued to be stable during the early stages of extensional deformation.

Many extensional microfractures and shear-band fabrics contain minerals such as chlorite and muscovite that indicate that mylonitic deformation continued through a range of progressively lower-grade metamorphic conditions during exhumation. Muscovite occurs locally at all structural levels, but overprinting of earlier fibrolite by coarse, patchy muscovite is most conspicuous in the mylonitic zone. Sample MP-HP12 is from the highest structural levels in the mylonitic zone and contains muscovite intergrown with biotite and fibrolite along shear bands and as blocky laths cutting across mylonitic foliation. We follow Hurlow et al. (1991) in the interpretation that the musco-

TABLE 3. SUMMARY OF THERMOCALC RESULTS

Sample	AJM-AL1			AJM-AL2	AJM-AL3			MP-AL311	MP-AL312	AJM-SC2
Deletions?	Paragonite			N.A.	Celadonite			N.A.	N.A.	N.A.
$X(H_2O)$	0.75	0.25	**Ind.**	**Ind.**	**0.75**	0.25	Ind.	**Ind.**	**Ind.**	**Ind.**
N_R	7	7	**6**	**3**	**7**	7	6	**4**	**4**	**6**
cor	0.927	0.917	**0.744**	**0.828**	**0.785**	0.762	0.848	**0.805**	**0.804**	**0.990**
fit	0.55	0.47	**0.51**	**0.58**	**0.30**	0.63	0.28	**0.04**	**0.88**	**1.30**
T (°C)	700°	606°	**630°**	**700°**	**672°**	591°	710°	**670°**	**630°**	**638°**
sd (*T*)	35°	27°	**105°**	**125°**	**22°**	18°	115°	**100°**	**90°**	**47°**
P (kbar)	5.8	5.0	**5.2**	**8.3**	**7.1**	6.5	7.4	**7.4**	**7.4**	**6.7**
sd (P)	1.3	1.1	1.4	1.2	0.7	0.6	1.2	1.2	1.1	1.0

Sample	AJM-WL1			AJM-WL2A			AJM-WL2B			MP-WL8A	AJM-WL3
Deletions?	N.A.			N.A.		Yes*	Na-phlogopite, hercynite			N.A.	N.A.
$X(H_2O)$	**0.75**	0.25	Ind.	**0.75**	0.25	Ind.	**0.75**	0.25	Ind.	**Ind.**	**Ind.**
N_R	**6**	6	5	**11**	11	6	**7**	7	6	**4**	**4**
cor	**0.709**	0.641	0.866	**0.824**	0.796	0.845	**0.890**	0.873	0.767	**0.738**	**0.802**
fit	**0.18**	0.49	0.20	**1.27**	1.60	0.30	**1.09**	1.46	0.68	**0.42**	**0.71**
T (°C)	**740°**	644°	740°	**650°**	585°	684°	**642°**	582°	795°	**645°**	**653°**
sd (*T*)	**50°**	38°	120°	**19°**	20°	59°	**23°**	27°	92°	**88°**	**96°**
P (kbar)	**8.4**	7.6	8.3	**6.1**	5.4	6.4	**6.1**	5.7	7.2	**6.3**	**7.0**
sd (*P*)	**0.9**	0.7	1.3	**0.4**	0.5	0.6	**0.8**	1.0	1.1	**1.0**	**1.0**

Sample	AJM-LB1			AJM-LB2	MP-LB132	MP-HP12			MP-AL196, Amphibolite symplectite		
Deletions?	N.A.			N.A.	Celadonite	N.A.			Hedenbergite		
$X(H_2O)$	**0.75**	0.25	Ind.	**Ind.**	**Ind**	0.75	0.25	**Ind.**	**0.75**	0.25	Ind.
N_R	**6**	6	5	**4**	**4**	6	6	**5**	**6**	6	5
cor	**0.762**	0.650	0.883	**0.818**	**0.708**	0.857	0.855	**0.761**	**0.595**	0.602	0.657
fit	**0.30**	0.57	0.34	**0.62**	**0.40**	0.41	0.32	**0.33**	**0.63**	0.62	0.71
T (°C)	**751°**	651°	754°	**717°**	**635°**	693°	602°	**632°**	**798°**	734°	752°
sd (*T*)	**54°**	40°	133°	**115°**	**106°**	39°	31°	**104°**	**49°**	42°	138°
P (kbar)	**8.6**	7.9	8.7	**8.0**	**5.9**	5.5	4.7	**5.0**	**9.5**	9.2	9.3
sd (*P*)	**0.9**	0.8	1.4	**1.2**	**0.9**	1.3	1.1	**1.4**	**1.0**	1.0	1.1

Note: N.A.—not applicable. Ind. indicates that the result is independent of or insensitive to water activity. Preferred results plotted in Figures 4 and 5 are indicated in boldface type. NR—number of reactions. The number of reactions determines the fit value necessary for 95% confidence. For NR = 3, fit = 1.96; NR = 4, fit = 1.73; NR = 5, fit = 1.61; NR = 6, fit = 1.54; NR = 7, fit = 1.49; NR = 11, fit = 1.37. The fit is a statistic derived from the c2 test expressing the goodness of fit of the data. All samples reported here pass the fit test at the 95% confidence level.

*Na-phlogopite, hercynite, spinel, and ilmenite deleted from the equilibrium assemblage.

vite in the mylonitic zone grew synkinematically with extension and overprinted older peak metamorphic assemblages that exceeded the second sillimanite isograd.

Potassium feldspar occurs most commonly in pelitic schists from deep structural levels, usually in small pods of intergrown K-feldspar, plagioclase, and quartz that probably represent neosome. Nevertheless, in at least one sample from relatively deep structural levels (AJM-AL1), orthoclase appears to be metamorphic rather than igneous in origin because it is intergrown with sprays of fibrolite separating muscovite from quartz, thus documenting that peak metamorphism reached the second sillimanite isograd.

In addition to the typical pelitic assemblages already discussed, two large blocks near Winchell Lake yield much more aluminous assemblages than other rocks observed in the East Humboldt Range (samples AJM-WL2A, AJM-WL2B). Sample MP-WL8A comes from the same locality but contains quartz, unlike the other two samples, which are undersaturated in silica. Unfortunately, these blocks may not be in place. The composite assemblage in samples AJM-WL2A and AJM-WL2B includes garnet + biotite + gedrite + staurolite + plagioclase + cordierite + hercynite + rutile + ilmenite + corundum ± fibrolite ± chlorite ± högbomite. Garnets in these rocks form large, complexly zoned porphyroblasts 1–2.5 cm in diameter and contain inclusions defining an early subassemblage of garnet + staurolite + gedrite + biotite + plagioclase + rutile + ilmenite. There are no constraints on when this subassemblage grew, but we suggest that it could have grown during the Late Cretaceous metamorphism. Inclusion trails define both straight and folded internal foliation with no systematic relationship to external foliation.

Some staurolite inclusions in garnet are idioblastic, but others show coronas of plagioclase separating staurolite from garnet. In addition, staurolite porphyroblasts in the matrix are commonly replaced by symplectites of cordierite + hercynite (AJM-WL2A) or plagioclase + hercynite + högbomite (AJM-WL2B) (Fig. 2C), suggesting reactions such as

$$5 \text{ grossular} + 2 \text{ Fe-staurolite} = 15 \text{ anorthite} + 8 \text{ hercynite} + 4\ H_2O \quad (dP/dT = 0.024 \text{ kbar/°C}) \qquad (4)$$

$$2 \text{ Mg-staurolite} = 3 \text{ cordierite} + 2 \text{ spinel} + 10 \text{ corundum} + 4\ H_2O \quad (dP/dT = 0.019 \text{ kbar/°C}) \qquad (5)$$

$$8 \text{ Fe-staurolite} + 6 \text{ anthophyllite} = \text{almandine} + 21 \text{ cordierite} + 29 \text{ hercynite} + 22\ H_2O \quad (dP/dT = 0.019 \text{ kbar/°C}). \qquad (6)$$

Locally, orthoamphibole is also fringed by cordierite, consistent with reaction 6. Staurolite is stable on the higher-pressure side of each of these reactions, so the moderate dP/dT of reactions such as 4 to 6 suggests a steeply decompressional *P-T* path.

Another reaction texture evident in sample AJM-WL2B involves the replacement of gedrite in the matrix by intergrowths of biotite and sparse, fine-grained fibrolite. In sample AJM-WL2A, gedrite survives only as inclusions in garnet, apparently having been completely replaced by biotite in the matrix. As in the amphibolites replaced by biotite in the Lizzie's Basin migmatite complex, the replacement of gedrite by biotite requires hydration and metasomatic introduction of potassium. Therefore, we speculate that much of the biotite and sillimanite grew during the same late-stage, H_2O-rich metamorphic event that produced the hydrous assemblages of the Lizzie's

Basin migmatite complex discussed earlier. Finally, chlorite commonly grows with fibrolite and biotite in still later veins.

QUANTITATIVE THERMOBAROMETRY

Approach

The results presented herein were obtained by using the Thermocalc computer program of Powell and Holland (1988) and the internally consistent thermodynamic database of Holland and Powell (1998). Complete tables of Thermocalc results are available from the GSA Data Repository (see text footnote 1) for all of the samples reported here plus four samples that did not yield meaningful results. These tables include lists of mineral end members, activities, reactions, and statistical details. Although we report only the Thermocalc results here, conventional thermobarometry yields substantially similar results (Peters, 1992), as does the Inveq approach (Gordon, 1992; Gordon et al., 1994) based on the internally consistent thermodynamic data set of Berman (1988). Solution models used to calculate activities follow Berman (1990) for garnet, Holland and Powell (1992) for plagioclase, Blundy and Holland (1990) for amphibole, Chatterjee and Flux (1986) for muscovite, and ideal mixing on sites (Powell, 1978) for biotite, clinopyroxene, cordierite, staurolite, hercynite-spinel, sphene, and ilmenite. Sillimanite, quartz, and rutile are treated as pure end members.

The thermodynamic data set of Holland and Powell (1998) was constructed by using least-squares analysis of experimental reversals and also natural partitioning data for the phases included in the data set. The result is an internally consistent set of enthalpies of formation with uncertainties. The other thermodynamic properties (entropy, volume, etc.) are regarded as known. By using appropriate solution models for participating phases, it is possible to use these data to calculate the positions of a complete set of linearly independent reactions for a specific metamorphic mineral assemblage given the compositions of the minerals participating in the reactions. Thermocalc offers two principle advantages: (1) it allows an appraisal of uncertainties in a given *P-T* estimate, and (2) it tests the internal consistency between all equilibria in a given assemblage, yielding a *P-T* estimate based on all available thermodynamic constraints for that assemblage.

Three principle sources of uncertainty factor into *P-T* estimates derived by this approach: (1) uncertainties in thermodynamic parameters of the participating phases (especially enthalpy), (2) uncertainties in the solution properties (i.e., activity models) of variable-composition phases, and (3) analytical uncertainties in microprobe

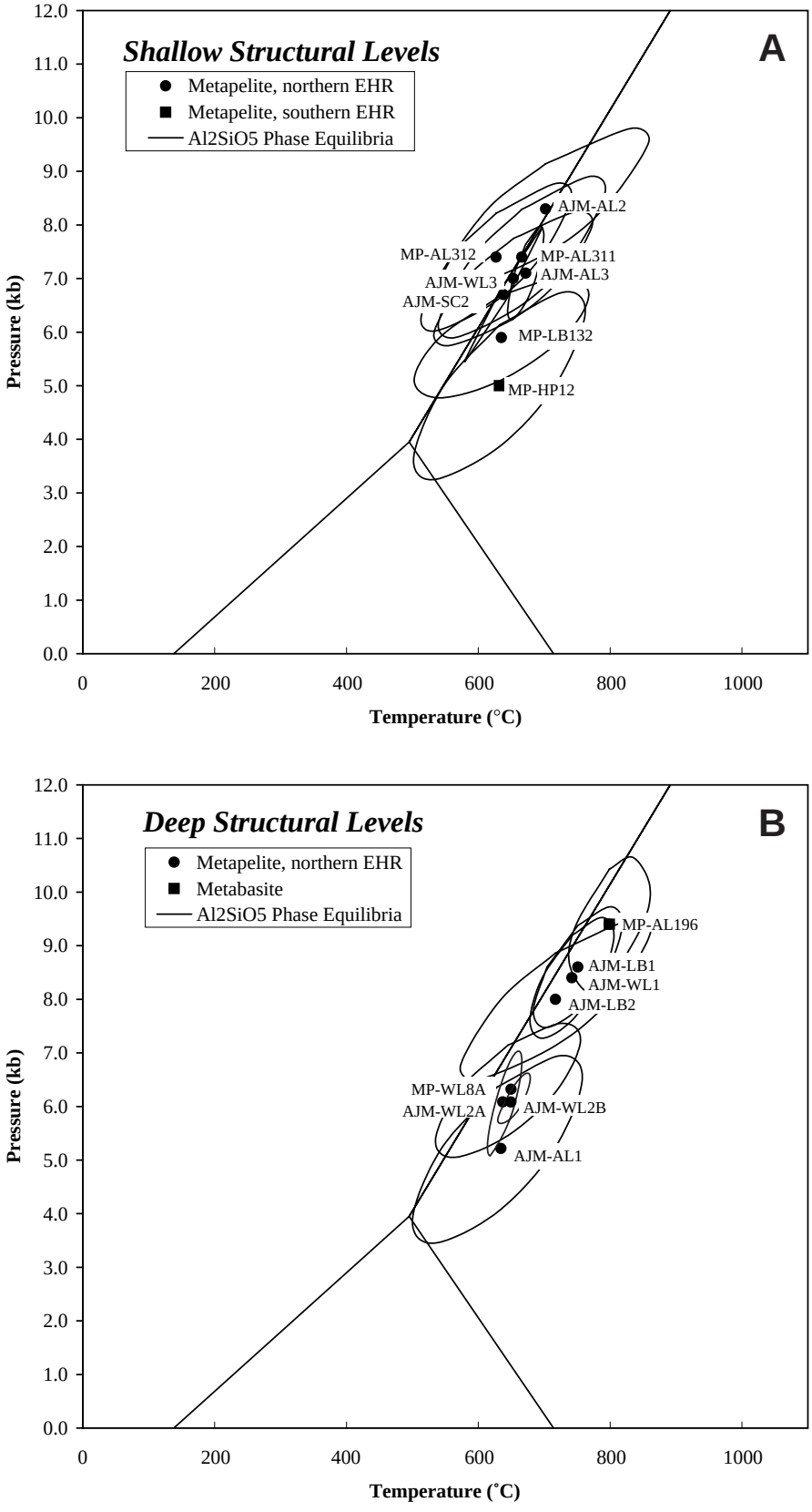

Figure 4. Pressure vs. temperature estimates with error ellipses from the East Humboldt Range based on the internally consistent data set of Holland and Powell (1990). (A) Results from relatively shallow structural levels. (B) Results from relatively deep structural levels.

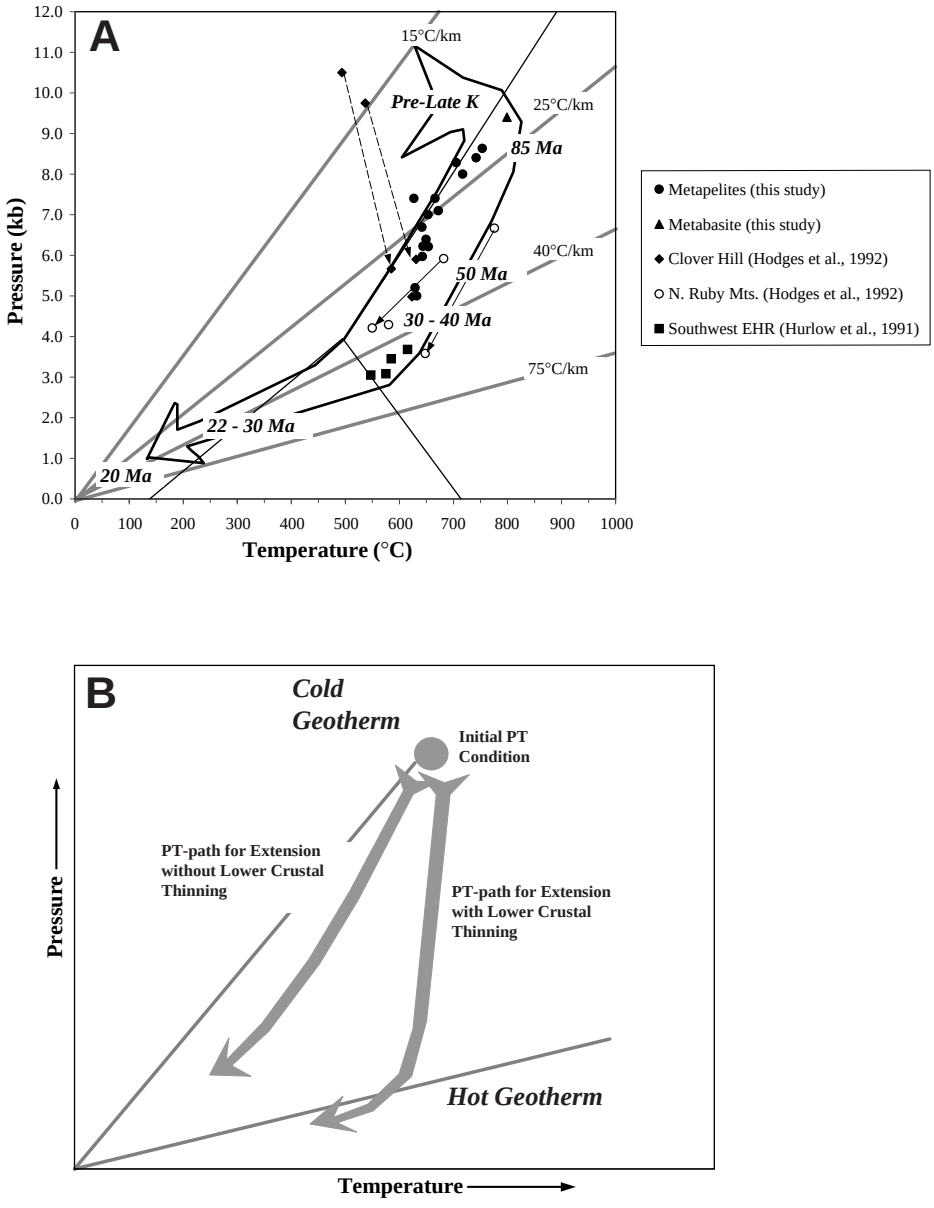

Figure 5. Interpretative diagrams of *P-T* results from the Ruby–East Humboldt metamorphic core complex. (A) Synoptic diagram of *P-T* results reported here combined with previously published results from elsewhere in the Ruby–East Humboldt metamorphic core complex (Hurlow et al., 1991; Hodges et al., 1992). Error ellipses have been left off to simplify viewing. The large open arrow shows the general *P-T-t* path inferred for the East Humboldt Range from late Mesozoic time to ca. 20 Ma based on the integration of *P-T* data with thermochronometric constraints (Dallmeyer et al., 1986; Dokka et al., 1986; McGrew and Snee, 1994). Shaded lines represent reference geotherms of 15, 25, 40, and 75 °C/km. The modern-day geothermal gradient in the Basin and Range province is ~25 °C/km, whereas the Battle Mountain heat-flow high is characterized by geothermal gradients on the order of 40–75 °C/km. Stability fields of the Al_2SiO_5 polymorphs are included for reference (Holdaway, 1971). (B) Schematic diagram illustrating expected *P-T-t* paths for uniform extension (with thinning of the lower crust) vs. nonuniform extension (without thinning of lower crust) (England and Jackson, 1987). Note the similarity of the inferred *P-T-t* path in Figure 5A to the model path expected for areas undergoing extension and lower-crustal thinning.

analyses of mineral compositions. Systematic uncertainties in thermodynamic parameters and in activity models give rise to large absolute uncertainties in *P-T* estimates, but do not contribute greatly to relative uncertainties between samples because relevant data are the same for all samples. Thermocalc provides a default formulation for uncertainties on activities that incorporates reasonable uncertainties in electron-microprobe data as well as uncertainties in the Margules parameters for nonideal mixing in solid-solution phases (Powell and Holland, 1988). Error propagations for this study were conducted as described for the calculation of relative uncertainties by Powell and Holland (1988). It should be noted that this approach yields stated uncertainties that are more conservative than many reported in the literature.

Certain equilibria (e.g., exchange reactions) tend to continue operating at lower temperatures than others (e.g., net transfer reactions) (Frost and Chacko, 1989). Thermocalc facilitates assessments of equilibrium in a given sample based on how well the calculated equilibria agree given probable magnitudes of relative uncertainty. By providing best-fit estimates of the *P-T* conditions at which each phase equilibrated as well as an average *P-T* for the entire assemblage, Thermocalc helps to identify those phases that may not be in equilibrium with the rest of the assemblage. In addition, Thermocalc offers a statistical test referred to as the "fit" that permits evaluation of whether the average *P-T* estimate is internally consistent within 95% confidence levels (Powell and Holland, 1988). Failure of the fit test probably implies a poorly equilibrated assemblage. In practice, the uncertainty in *P-T* estimates for a given rock primarily reflects the number of equilibria, the angles at which they intersect, and the degree of internal consistency between equilibria. Estimates based on relatively few equilibria (e.g., three or four) or on equilibria that intersect at low angles nearly always yield large uncertainties regardless of how good the fit of the data is. Consequently, large stated uncertainties are not necessarily indicative of poor data quality but may merely reflect the number and angles of intersection of the equilibria. It is more important to consider the fit and the individual mineral diagnostics.

Because metamorphic equilibration is a diffusion-controlled process, it depends on time, temperature, and the grain size of the participating minerals. For example, at a temperature of 700 °C, garnets of the typical grain size observed in this study (radius = 0.4–2 mm) would require 1–20 m.y. to homogenize (following the approach of Muncill and Chamberlain, 1988, and using the diffusion coefficients of Cygan and Lasaga, 1985; see Peters, 1992, for detailed discussion). Consequently, most of the samples investigated here are unlikely to preserve

growth zoning, leading us to avoid applying the Gibbs method.

In deformed terranes such as the East Humboldt Range, processes such as dislocation creep and dynamic recrystallization may also enhance diffusion rates and thus facilitate reequilibration. Therefore, more strongly deformed rocks near the center of the mylonitic zone may reequilibrate under lower-grade conditions than less deformed rocks at deeper structural levels. Furthermore, microscopic deformation zones within a given thin section may not be in strict equilibrium with lower-strain domains. Naturally, the composition and abundance of any pore fluid also affect the equilibration of a given rock. Moreover, if pore fluids were channelized rather than pervasive, then fluid-rich domains are more likely to reequilibrate. Considering the scale of diffusion and the possibility of domainal reequilibration, we have been careful to base *P-T* estimates only on mineral-rim compositions of grains within narrowly defined domains that are not divided by shear bands. Although we believe this is an appropriately conservative approach in light of the possibility of disequilibrium between mineral cores, we note that the rim thermobarometric results reported here are best regarded as *minimum* estimates. Nevertheless, because rates of exhumation (and thus cooling) were probably high during Tertiary metamorphism, we expect that some of these rocks may record pressures and temperatures approaching peak-metamorphic conditions during Late Cretaceous to Tertiary time.

Results and Interpretation

Table 3 and Figure 4 summarize quantitative thermobarometric results from 15 metapelite samples and one metabasite from the East Humboldt Range. The preferred results plotted in Figure 4 are indicated in boldface type in Table 3. Sample localities are shown in Figure 1. All of the *P-T* estimates reported here yield internally consistent results that pass the statistical fit test. Rarely, it was necessary or desirable to delete poorly equilibrated mineral end members from the equilibrium assemblage in order to improve results (see Table 3).

A problem with the Thermocalc approach, as with other thermobarometric approaches, is how to treat water activities. In several samples, this is not an issue because only fluid-independent equilibria could be written for the given assemblage (i.e., samples AJM-AL2, MP-AL311, MP-AL312, AJM-SC2, MP-WL8A, AJM-WL3, AJM-LB2, and MP-LB132). For the remaining samples, it is possible to force Thermocalc to include only fluid-independent equilibria by deleting water from the equilibrium assemblage, and fluid-independent *P-T* estimates have been included for all samples in Table 3. However, this approach effectively discards the information potentially provided by water-sensitive equilibria, and because dehydration reactions tend to be good geothermometers, it commonly leads to excessively large uncertainties in temperature. Therefore, Table 3 also includes *P-T* estimates for a range of X_{H_2O} conditions for fluid-sensitive assemblages (usually $X_{H_2O} = 0.25$ and 0.75).

As shown in Table 3, increasing water activity invariably correlates with increasing temperature. If either temperature or fluid composition can be independently constrained, then it is possible to solve for the other as well. Peters and Wickham (1994) reported that metacarbonate and calc-silicate rocks from the East Humboldt Range preserve a high-temperature, water-rich ($X_{H_2O} \geq 0.8$) assemblage that overprints earlier assemblages, which also record high-temperature but more CO_2-rich conditions. Fluid composition may vary from place to place, but we infer that water-rich conditions probably accompanied metamorphism of the metapelitic rocks as well, especially since the temperature estimates derived from the water-rich metacarbonate assemblages overlap with those reported here.

A second test of this interpretation is provided by comparing the Thermocalc results with the garnet-biotite geothermometer. Although in theory the thermodynamics of the garnet-biotite system are already incorporated into Thermocalc, the Thermocalc approach tends to underweight this well-calibrated, fluid-independent geothermometer. In general, the Thermocalc temperature estimates reported here are only consistent with garnet-biotite temperatures when relatively water-rich conditions are assumed ($X_{H_2O} \geq 0.5$), thus providing an additional argument for the presence of a water-rich pore fluid. In addition, fluid-independent *P-T* estimates from Thermocalc itself are generally more compatible with the water-rich than with the water-poor results (Table 3). Accordingly, for most of the fluid-sensitive results reported here we prefer the *P-T* estimates based on relatively water-rich conditions ($X_{H_2O} \geq 0.75$) (shown in boldface type in Table 3 and plotted in Figure 4). Two exceptions to this generalization are samples AJM-AL1 and MP-HP12, both of which yield relatively lower garnet-biotite and fluid-independent temperature estimates, which may be consistent with less water-rich conditions. Accordingly, for these two samples we have accepted the less tightly constrained but more conservative fluid-independent results for the preferred *P-T* estimates plotted in Figure 4.

Regardless of how water activities are treated, the *P-T* estimates reported here define an approximately linear trend from >9 kbar and 800 °C to 5 kbar and 630 °C (Table 3, Fig. 4). This linear trend does not represent a simple metamorphic field gradient because the *P-T* estimates vary from locality to locality without defining a systematic geographic pattern. Furthermore, the same general data trend is evident at both high and low structural levels (Fig. 4, A and B). Another possible interpretation is that the results represent artifacts of frozen-in diffusion profiles in disequilibrium. Although this viewpoint may have some merit, several lines of evidence lead us to believe that many of these samples are relatively well equilibrated. As previously discussed, the statistics associated with Thermocalc allow an appraisal of the internal consistency between different equilibria operating in a given rock. All of the results reported here pass the fit test using mineral-rim compositions, and most give statistically quite robust results. Moreover, mineral rims on the scale of a thin section tend to be quite homogeneous compositionally, and in many instances garnet porphyroblasts show broad, relatively flat zoning profiles that probably record diffusional reequilibration. In general, *P-T* estimates based on garnet cores are either statistically similar to those based on rims or are less statistically robust than the rim results. Therefore, we infer that the spread in *P-T* results reflects diachronous equilibration of samples on a relatively local scale at different points along a steeply decompressional *P-T* path. Such local variability in timing of equilibration could reflect differences in grain size, deformation rate, or fluid activity between sample localities. As subsequently outlined in detail, our favored interpretation is that the steeply inclined *P-T* trend from the East Humboldt Range records decompressional metamorphism accompanying exhumation between Late Cretaceous and late Oligocene time. This interpretation does not stand on its own, but rather is built on the petrographic and geochronological relationships described herein and a well-defined tectonic context for late Mesozoic to Cenozoic time.

The critical issue in the interpretation of these results is the timing of equilibration of the rim *P-T* estimates. As discussed previously, we argue that a Late Cretaceous U-Pb zircon date on leucogranite from the hinge zone of the Winchell Lake nappe constrains the age of a major phase of metamorphism, migmatization, and nappe emplacement. Similar Late Cretaceous U-Pb dates have been reported on zircon from leucogranite in the southern East Humboldt Range and on monazites from leucogranite and pelitic schist from the northern Ruby Mountains (Snoke et al., 1979, 1992; J. E. Wright, A. W. Snoke, and K. A. Howard, unpublished data). In light of the high-grade and regional extent of this metamorphism, the *P-T* results reported here probably do not predate the Late Cretaceous. In addition, most of the mineral assemblages reported here include phases

such as sillimanite and muscovite that grew during or after the Late Cretaceous metamorphism. Therefore, we infer that the Late Cretaceous dates provide an older age limit for the timing of all *P-T* estimates reported here.

The younger age limit for metamorphic equilibration in the East Humboldt Range hinges on $^{40}Ar/^{39}Ar$ hornblende cooling ages from the central and northern part of the range. Temperature estimates of 640–800 °C for pelitic assemblages in the northern half of the East Humboldt Range are well above nominal closure temperatures for $^{40}Ar/^{39}Ar$ dating of hornblende (480–580 °C) (Harrison and McDougall, 1980). Therefore, $^{40}Ar/^{39}Ar$ hornblende cooling ages define a younger age limit for the *P-T* estimates reported here. For samples collected at relatively shallow structural levels (corresponding to elevations above ~2930 m [~9600 ft] in Table 2), the younger age limit is given by hornblende cooling ages between 50 and 63 Ma, whereas early Oligocene hornblende cooling ages of 30–36 Ma define the younger age limit at deeper levels (McGrew and Snee, 1994).

P-T estimates from shallow structural levels (samples AJM-AL2, MP-AL311, MP-AL312, AJM-AL3, AJM-SC2, AJM-WL3, and MP-LB132) are in the ranges of 6 to 8.5 kbar and 630 to 700 °C (Fig. 4A). These results are bracketed within a 20–30 m.y. time interval from Late Cretaceous to early Eocene, and the range in pressures suggests that decompression of 2 to 3 kbar could have occurred during this interval. Textural evidence supports this possibility. For instance, one sample preserves relict kyanite mantled by sillimanite, implying that the rocks passed from the kyanite to the sillimanite stability field before 84 Ma (see Petrography, Phase Relationships, and Mineral Chemistry). Other samples show assemblages that were at least partly synkinematic with extensional shear fabrics, such as late-stage muscovite growing along extensional shear bands. This textural relationship suggests that muscovite became stable during the course of extensional exhumation (see also Hurlow et al., 1991). Consequently, we suggest that rim equilibration at high structural levels occurred at different points along a steeply decompressional *P-T* path extending from ~8.5 kbar to <6 kbar during Late Cretaceous to early Tertiary time. These results fortify previously published suggestions that unroofing of the northern part of the Ruby Mountains and East Humboldt Range began as early as Eocene or even Late Cretaceous time (Hodges et al., 1992; McGrew and Snee, 1994).

P-T results from deeper structural levels are less tightly clustered both in terms of the range of *P-T* conditions and the age brackets (cf. samples AJM-AL1, AJM-WL1, AJM-WL2A, AJM-WL2B, MP-WL8A, AJM-LB1, AJM-LB2, and amphibolite sample MP-AL196) (Fig. 4B). Results from deep structural levels range from 5 to 9.4 kbar and 630 to 800 °C. The broad range of *P-T* conditions inferred for these samples implies that they did not equilibrate simultaneously. The samples yielding the higher-pressure results may have equilibrated during Late Cretaceous or early Tertiary time as discussed previously, but the lower-pressure results could record conditions during Oligocene metamorphism and deformation. Samples AJM-AL1, AJM-WL2A, AJM-WL2B, and MP-WL8A are the best candidates for early Oligocene equilibration. Not only do they record relatively low pressures of equilibration, but they also display a variety of reaction textures indicating a steeply decompressional *P-T* path, consistent with rapid extensional unroofing (see Petrography section). The increasing Tertiary thermal overprint at depth in the northern East Humboldt Range may help explain why some samples at deep structural levels reequilibrated during Tertiary metamorphism.

In general, the *P* and *T* values reported herein from the northern East Humboldt Range are distinctly higher than previously published results from the southern East Humboldt Range (Hodges et al., 1992; Hurlow et al., 1991). However, one of the samples reported here, sample MP-HP12, comes from the southern part of the range and yields a *P-T* estimate (5.0 ± 1.4 kbar, 632 ± 104 °C) that statistically overlaps the previously published results of Hurlow et al. (1991) (Fig. 5A). As noted in the Petrography section, muscovite in sample MP-HP12 is texturally late, growing in or even cutting mylonitic foliation. Consequently, we think that the *P-T* estimate reported here, with muscovite included in the equilibrium assemblage, offers a robust estimate of metamorphic conditions during one stage of Tertiary mylonitic deformation. This interpretation reinforces the earlier interpretation of Hurlow et al. (1991). We note that recalculating the data reported by Hurlow et al. (1991) using the Thermocalc approach does not significantly change their results, nor does recalculating our *P-T* estimates using their approach significantly change the results reported here (Peters, 1992). Therefore, the lower pressures obtained from the southern East Humboldt Range are not merely an artifact of the difference in approach. Enhanced diffusion rates due to grain-size reduction, more active pore fluids, or higher rates of dynamic recrystallization and dislocation creep in these rocks may have facilitated reequilibration at lower *P-T* conditions.

Sample MP-AL196, the only metabasite investigated here, is a garnet amphibolite collected at intermediate structural levels on the north side of Angel Lake cirque. Mineral rims and symplectite phases yield quite similar *P-T* results of ~800 °C and 9.5 kbar (Table 3, Fig. 4). This result lies at the top of the data trend defined by the results from the metapelitic rocks, suggesting that the amphibolite assemblage may have "frozen in" at an earlier stage in the cooling history than most of the metapelites.

One of the most important results from the metabasite assemblages emerges not from the quantitative thermobarometry but from the basic petrography. To wit, the relative abundance of garnet in these rocks combined with the widespread development of decompressional reaction textures strongly supports the thesis of an early, relatively high-pressure metamorphism followed by further metamorphism along a steeply decompressional *P-T-t* path. The timing constraints on metamorphism of the amphibolites resemble those for the metapelitic assemblages already discussed. In particular, an $^{40}Ar/^{39}Ar$ hornblende cooling age of 51.0 ± 2 Ma on an amphibolite collected ~150 m upslope from MP-AL196 provides a reasonable minimum age estimate for the timing of metamorphism (McGrew and Snee, 1994). Consequently, the detailed petrography of this sample strongly supports the inference that decompression of the East Humboldt Range began by early Eocene time.

DISCUSSION AND TECTONIC IMPLICATIONS

The thermobarometric results reported herein define an elongate field nearly parallel to the kyanite = sillimanite join, from >9 kbar and 800 °C to ~5 kbar and 630 °C (Figs. 4, 5A). These results reinforce previously published *P-T* estimates of ≥6 kbar and 550–750 °C based on calc-silicate assemblages (Peters and Wickham, 1994). As discussed, we believe that the trend of *P-T* results from the northern part of the range defines a *P-T-t* path for Late Cretaceous to Oligocene time, yielding a decompressional cooling trajectory of ~40 °C/kbar (~11 °C/km) (Fig. 5A). This steep *P-T-t* path implies that unroofing outpaced cooling, a scenario consistent with rapid exhumation, most likely as a product of post–85 Ma tectonic denudation. We emphasize that this inferred *P-T-t* path is based not only on quantitative *P-T* results, but also on decompressional reaction textures, synkinematic mineral growth relative to extensional microstructures, and integration with available thermochronologic constraints. In addition, the *P-T-t* path favored here resembles that suggested for the northern Ruby Mountains by Hodges et al. (1992) on the basis of Gibbs method modeling of garnet zoning profiles (Fig. 5A).

We therefore suggest that tectonic denudation of the Ruby–East Humboldt terrane probably began during the late stages or immediately after the Late Cretaceous Sevier orogeny. In particular,

$^{40}Ar/^{39}Ar$ hornblende cooling ages of 50–63 Ma imply that decompressional metamorphism at high structural levels in the northern East Humboldt Range began by early Eocene or perhaps even Late Cretaceous time (McGrew and Snee, 1994). Furthermore, synkinematic relationships with extensional microstructures directly link this decompressional *P-T-t* path to extensional shearing, thus providing a direct link between early Tertiary unroofing and activity on the major extensional shear system that exhumed the East Humboldt Range from depths of at least 30 km.

These results add to a growing body of evidence suggesting that regional extension began by early Tertiary or perhaps even Late Cretaceous time. Other lines of evidence that support an Eocene or older age for the onset of regional extension in northeastern Nevada include (1) the existence of a detachment fault capped by middle Eocene volcanic rocks in the Pequop Mountains (Camilleri, 1992) and a detachment fault cut by latest Eocene plutonic rocks in the Pilot Range (Miller et al., 1987), (2) the identification of early Tertiary sedimentary basins that were probably related to contemporaneous regional extension (Mueller and Snoke, 1993; Brooks et al., 1995; Potter et al., 1995), and (3) the discovery that by Eocene time, the southeastern Wood Hills had cooled through $^{40}Ar/^{39}Ar$ biotite closure temperatures (~300 °C) following Mesozoic metamorphism at conditions of 550–625 °C and 5–6.4 kbar (18–24 km) (Thorman and Snee, 1988; Hodges et al., 1992; Camilleri and Chamberlin, 1997). Finally, early Tertiary extension broadly coincides with exhumation of the metamorphic core complexes to the north of the Snake River Plain (e.g., Carr et al., 1987; Silverberg, 1990; Berger and Snee, 1992).

Nevertheless, we note that the existence of large, surface-breaking normal faults in the Sevier hinterland has not been proven for time periods before the middle Eocene, and until such faults are discovered, at least three alternative models remain viable that could produce partial deep-crustal unroofing without regional crustal extension. The first alternative model is partial unroofing due to surface erosion. Even though impossible to preclude at present, this mechanism appears to be unlikely because of (1) the lack of a complementary large depositional center of Late Cretaceous age and (2) the difficulty of explaining why some areas were so denuded while extensive nearby areas still preserve unmetamorphosed sedimentary sequences as young as Triassic in age. The second viable model for unroofing is the gravity-current hypothesis of Wernicke and Getty (1997). In this model, development of a low-density deep-crustal root during tectonic shortening induces redistribution of mass in the deeper crust by spreading of the hot, weak, buoyant root zone with or without corresponding extension at upper-crustal levels. A third, somewhat similar unroofing model is diapiric uplift of buoyant, partially molten, deep-crustal infrastructure (e.g., Armstrong and Hansen, 1966; Howard, 1980). Although the gravity-current and diapiric-uplift models cannot bring deep-crustal rocks to the surface, they do provide viable mechanisms by which rocks can move from deep-crustal to mid-crustal levels, as observed in the East Humboldt Range. The three models cannot be discriminated by *P-T-t* paths alone, but rather require reconstruction of deformation patterns at all structural levels through the Late Cretaceous–early Tertiary crust of the hinterland of the Sevier orogenic belt. At present the post-Eocene extensional tectonic overprint obscures the critical relationships.

Regardless of earlier tectonic history, high-grade conditions persisted as extensional exhumation proceeded, as evidenced by (1) early Oligocene $^{40}Ar/^{39}Ar$ hornblende cooling ages from deep structural levels in the northern East Humboldt Range (Dallmeyer et al., 1986; McGrew and Snee, 1994), (2) quartz crystallographic textures characteristic of upper-amphibolite-facies to granulite-facies deformation (McGrew and Casey, 1998), (3) microstructures commonly associated with amphibolite-grade deformation in 40 and 29 Ma orthogneisses (McGrew, 1992), and (4) *P-T* estimates of 3–5 kbar and 550–650 °C for extensional mylonitization in the northern Ruby Mountains and East Humboldt Range (Hurlow et al., 1991; Hodges et al., 1992). The new petrographic and thermobarometric results reported here support these interpretations of the high-grade nature of Tertiary mylonitic deformation. Important new petrographic evidence includes the existence of high-grade decompressional reaction textures (e.g., samples MP-AL196, AJM-WL2, and MP-WL8A) and the growth of high-grade mineral assemblages in steeply dipping veins and normal-sense shear bands. Sample MP-HP12 yields a *P-T* estimate of 5 kbar and 630 °C based on assemblages that are at least partly synkinematic with mylonitic deformation (Table 3, Fig. 5A). Sample AJM-AL1 (630 °C, 5 kbar) may also record middle Tertiary conditions on the basis of its relatively low pressures and the fact that other rocks from similar structural levels preserve early Oligocene $^{40}Ar/^{39}Ar$ hornblende cooling ages.

Finally, we consider what these results may imply about the character and evolution of the thermal structure of the crust through the course of extensional tectonism. Assuming that the *P-T* results are reasonably accurate in an absolute sense, then the upper end of the inferred *P-T-t* path plots very near the average geotherm of the modern Basin and Range province (~25 °C/km), but the lower end plots along an exceptionally steep geothermal gradient resembling that of the Battle Mountain area today (>40 °C/km) (Lachenbruch and Sass, 1978) (Fig. 5A). The Battle Mountain heat-flow high is an area of steep geothermal gradients located immediately northwest of the Ruby Mountains and East Humboldt Range today, and the Marys River fault—a possible contemporary analogue of the Ruby–East Humboldt detachment system—roots in that direction. It is possible that a metamorphic core complex could be forming today in the deep-crustal root zone of this large, probably active fault system, helping to explain the anomalously high modern heat flow.

The *P-T* evolution from a shallower to a steeper geotherm implies that the rocks tended to carry isotherms upward with them during the early phases of extensional exhumation, much as predicted by England and Jackson (1987) for uniformly extending lithosphere (Fig. 5B). In this context, we note that the vast majority of unroofing was accomplished well before the rocks approached $^{40}Ar/^{39}Ar$ mica and fission-track cooling ages, again as predicted by England and Jackson (1987) for uniform extension of the lithosphere (Fig. 5B). Consequently, the rapid cooling through the lower-temperature part of the time-temperature path does not necessarily record extreme rates of exhumation, but may merely reflect reestablishment of a more normal geothermal gradient during the final stages of extensional tectonic exhumation (McGrew and Snee, 1994).

CONCLUSIONS

Metamorphic rocks in the northern East Humboldt Range preserve a classic clockwise *P-T* loop that began before Late Cretaceous time (possibly during the Late Jurassic?) with deep-crustal tectonic burial to depths of >30 km recorded by growth of a kyanite + garnet ± staurolite subassemblage. Late Cretaceous metamorphism overprinting this older event reached the second sillimanite isograd and involved the growth of abundant sillimanite at the expense of earlier kyanite. This initial phase of sillimanite-grade metamorphism accompanied emplacement of the Winchell Lake nappe and was synchronous with leucogranite generation dated at 84.8 ± 2.8 Ma. This new date forges a vital link between magmatism, metamorphism, and large-scale deep-crustal flow in the hinterland of the Sevier orogenic belt during Late Cretaceous time. *P-T* estimates of >9 kbar and 800 °C may date from this time, but in any case must predate cooling of high structural levels through $^{40}Ar/^{39}Ar$ hornblende closure temperatures at 50–63 Ma (McGrew and Snee, 1994).

In conjunction with previously published results, the *P-T* results reported here define a linear field with a slope of ~40 °C/kbar in *P-T* space. Textural relationships suggest that most of the *P-T* estimates probably record diachronous metamor-

phism along a steeply decompressional *P-T-t* path accompanying early to middle Tertiary extensional deformation. We argue that the variation in *P-T* estimates along this trend reflects localized variability in the timing of thermobarometric closure due to spatial variations in parameters such as grain size, strain rate, or fluid activity between outcrops. If correct, then this trend records a *P-T* path for tectonic unroofing of the Ruby Mountains and East Humboldt Range. Integrating the *P-T* data with $^{40}Ar/^{39}Ar$ hornblende cooling ages from high structural levels implies that >2.5 kbar of decompression probably occurred before middle Eocene time (equivalent to at least 9 km of unroofing). In light of the new constraints on the age of the Winchell Lake nappe, these results indicate that the deeper crust between the Sevier belt and the Sierra Nevada arc was thermally weakened and actively flowing between Late Cretaceous and early Eocene time. We suggest that thermal softening of the crust may have triggered partial tectonic denudation of the hinterland beginning as early as Late Cretaceous time. Regional gravitational collapse, gravity currents, and diapiric upwelling of a buoyant, mobile, partially molten, deep-crustal layer are all viable hypotheses for this early stage in the unroofing history.

A *P-T* estimate of ~5 kbar and 630 °C represents a plausible value for extensional mylonitization in the southern part of the range, in general agreement with earlier reported results (Hurlow et al., 1991). Relatively deep structural levels in the northern part of the range may also have been subjected to *P-T* conditions of 5 kbar and 630 °C in early Oligocene time.

The steep *P-T* path delineated here implies a thermal evolution from a shallower to a steeper geotherm during extensional exhumation, probably because of the combined effects of plastic stretching of the lower plate and thinning and removal of the upper plate (cf. England and Jackson, 1987). The rocks of the East Humboldt Range may have started near a typical Basin and Range province geotherm of ~25 °C/km before middle Eocene time, but as exhumation proceeded, the thermal regime evolved to a much steeper geotherm resembling the present-day Battle Mountain heat-flow high.

These results imply that the crust was in an anomalously hot, weak state during core-complex development. If geothermal gradients this steep were maintained long enough, then plastic deformation could have persisted to levels as shallow as 5–7 km in the crust, promoting a thin seismogenic zone and a relatively flexible upper-crustal layer. Meanwhile, much of the deeper crust would have been at or near melting conditions, consistent with the existence of a thick, asthenosphere-like deep-crustal layer during core-complex evolution (e.g., Gans, 1987; Wernicke, 1990; Kruse et al., 1991; MacCready et al., 1997). The combination of a thin, flexible upper crust with a weak, flowing deeper crust would have created a dynamic coupling that may be a crucial ingredient in development of metamorphic core complexes. In this view, large-displacement, rolling-hinge-style exhumation of the core complex would have been enabled by tight isostatic flexure of the thermally weakened crust. Meanwhile, motion on the detachment fault itself would promote and sustain the necessary steep geothermal gradients while simultaneously imposing the differential gravitational loads that drive compensatory flow at deeper levels.

ACKNOWLEDGMENTS

This research was partially supported by National Science Foundation grants EAR 87-20097 and EAR 90-19256 to Steve Wickham, National Science Foundation grant EAR 87-07435 to A. W. Snoke, a Geological Society of America Penrose Graduate Student Research grant to Mark T. Peters, and graduate assistantships from the University of Wyoming and the University of Chicago. This paper is a combination of work done by Allen J. McGrew and Mark T. Peters as part of their Ph.D. dissertations at the University of Wyoming and the University of Chicago, respectively, who especially thank their Ph.D. advisors, Art Snoke and Steve Wickham, for support and insights throughout the course of this study. In addition, we thank Judy Baker, Phyllis Camilleri, Ron Frost, Kip Hodges, Bob Newton, Zeke Snow, and Geoff Nichols for valuable discussions. David Applegate, Kip Hodges, and Tom Hoisch greatly improved the manuscript with insightful formal reviews. Sue Swapp and Tony Hoch at the University of Wyoming, Karl Hager at Purdue University, and Ian Steele at the University of Chicago provided valuable technical assistance with the electron microprobes. Allen McGrew also thanks the Department of Geology at Purdue University for making its electron-microprobe facility available and thus greatly facilitating completion of this project.

REFERENCES CITED

Armstrong, R. L., and Hansen, E., 1966, Cordilleran infrastructure in the eastern Great Basin: American Journal of Science, v. 264, p. 112–127.

Berger, B. R., and Snee, L. W., 1992, Thermochronologic constraints on mylonite and detachment fant development, Kettle Highlands, northeastern Washington and southern British Columbia: Geological Society of America Abstracts with Programs, v. 24, no. 7, p. 65.

Berman, R. G., 1988, Internally-consistent thermodynamic data for minerals in the system Na_2O-K_2O-CaO-MgO-FeO-Fe_2O_3-Al_2O_3-SiO_2-TiO_2-H_2O-CO_2: Journal of Petrology, v. 29, p. 445–522.

Berman, R. G., 1990, Mixing properties of Ca-Mg-Fe-Mn garnets: American Mineralogist, v. 75, p. 328–344.

Blundy, J. D., and Holland, T. J. B., 1990, Calcic amphibole equilibria and a new amphibole-plagioclase geothermometer: Contributions to Mineralogy and Petrology, v. 104, p. 208–224.

Brooks, W. E., Thorman, C. H., and Snee, L. W., 1995, The $^{40}Ar/^{39}Ar$ ages and tectonic setting of the middle Eocene northeast Nevada volcanic field: Journal of Geophysical Research, v. 100, p. 10403–10416.

Camilleri, P. A., 1992, Mesozoic structural and metamorphic features in the Wood Hills and Pequop Mountains, northeastern Nevada, *in* Wilson, J. R., ed., Field guide to geologic excursions in Utah and adjacent areas of Nevada, Idaho, and Wyoming: Utah Geological and Mineral Survey Miscellaneous Publication 92–3, p. 93–105.

Camilleri, P. A., and Chamberlin, K. R., 1997, Mesozoic tectonics and metamorphism in the Pequop Mountains and Wood Hills region, northeast Nevada: Implications for the architecture and evolution of the Sevier orogen: Geological Society of America Bulletin, v. 109, p. 74–94.

Carr, S. D., Parrish, R., and Brown, R. L., 1987, Eocene structural development of the Valhalla complex, southeastern British Columbia: Tectonics, v. 6, p. 175–196.

Chatterjee, N. D., and Flux, S., 1986, Thermodynamic mixing properties of muscovite-paragonite crystalline solutions at high temperatures and pressures, and their geological applications: Journal of Petrology, v. 27, p. 677–693.

Cooper, A. F., 1972, Progressive metamorphism of metabasic rocks from the Haast Schist Group of southern New Zealand: Journal of Petrology, v. 13, p. 457–492.

Cygan, R. T., and Lasaga, A. C., 1985, Self-diffusion of magnesium in garnet at 750 to 900 °C: American Journal of Science, v. 285, p. 328–350.

Dallmeyer, R. D., Snoke, A. W., and McKee, E. H., 1986, The Mesozoic-Cenozoic tectonothermal evolution of the Ruby Mountains–East Humboldt Range, Nevada: A Cordilleran metamorphic core complex: Tectonics, v. 5, p. 931–954.

Dokka, R. K., Mahaffie, M. J., and Snoke, A. W., 1986, Thermochronologic evidence of major tectonic denudation associated with detachment faulting, northern Ruby Mountains–East Humboldt Range, Nevada: Tectonics, v. 5, p. 995–1006.

England, P., and Jackson, J., 1987, Migration of the seismic-aseismic transition during uniform and nonuniform extension of the continental lithosphere: Geology, v. 15, p. 291–294.

Frost, B. R., and Chacko, T., 1989, The granulite uncertainty principle: Limitations on thermobarometry in granulites: Journal of Geology, v. 97, p. 435–450.

Gans, P. B., 1987, An open-system, two-layer crustal stretching model for the eastern Great Basin: Tectonics, v. 6, p. 1–12.

Gordon, T. M., 1992, Generalized thermobarometry: Solution of the inverse chemical equilibrium problem using data for individual species: Geochimica et Cosmochimica Acta, v. 56, p. 1793–1800.

Gordon, T. M., Aranovich, L. Ya., and Fed'kin, V. V., 1994, Exploratory data analysis in thermobarometry: An example from the Kisseynew sedimentary gneiss belt, Manitoba, Canada: American Mineralogist, v. 79, p. 973–982.

Harrison, T. M., and McDougall, I., 1980, Investigations of an intrusive contact, northwest Nelson, New Zealand—I. Thermal, chronological and isotopic constraints: Geochimica et Cosmochimica Acta, v. 44, p. 1985–2003.

Hodges, K. V., Snoke, A. W., and Hurlow, H. A., 1992, Thermal evolution of a portion of the Sevier hinterland: The northern Ruby Mountains–East Humboldt Range and Wood Hills, northeastern Nevada: Tectonics, v. 11, p. 154–164.

Holdaway, M. J., 1971, Stability of andalusite and the aluminum silicate phase diagram: American Journal of Science: v. 271, p. 97–131.

Holland, T. J. B., and Powell, R., 1992, Plagioclase feldspars: Activity-composition relations based upon Darken's quadratic formalism and Landau theory: American Mineralogist, v. 77, p. 1413–1424.

Holland, T. J. B., and Powell, R., 1998, An internally consistent thermodynamic data set for phases of petrological interest: Journal of Metamorphic Geology, v. 16, p. 309–343.

Hollister, L. S., 1966, Garnet zoning: An interpretation based on the Rayleigh fractionation model: Science, v. 154, p. 1647–1651.

Howard, K. A., 1980, Metamorphic infrastructure in the northern Ruby Mountains, Nevada, *in* Crittenden, M. D., Jr., Coney, P. J., and Davis, G. H., eds., Cordilleran metamorphic core complexes: Geological Society of America Memoir 153, p. 335–347.

Hudec, M. R., 1990, The structural and thermal evolution of the central Ruby Mountains, Elko County, Nevada [Ph.D. dissert.]: Laramie, University of Wyoming, 272 p.

Hudec, M. R., 1992, Mesozoic structural and metamorphic history of the central Ruby Mountains metamorphic core complex, Nevada: Geological Society of America Bulletin, v. 104, p. 1086–1100.

Hudec, M. R., and Wright, J. E., 1990, Mesozoic history of the central part of the Ruby Mountains–East Humboldt Range metamorphic core complex, Nevada: Geological Society of America Abstracts with Programs, v. 22, no. 3, p. 30.

Hurlow, H. A., Snoke, A. W., and Hodges, K. V., 1991, Temperature and pressure of mylonitization in a Tertiary extensional shear zone, Ruby Mountains–East Humboldt Range, Nevada: Tectonic implications: Geology, v. 19, p. 82–86.

Kistler, R. W., Ghent, E. D., and O'Neill, J. R., 1981, Petrogenesis of garnet two-mica granites in the Ruby Mountains, Nevada: Journal of Geophysical Research, v. 86, p. 10591–10606.

Kohn, M. J., and Spear, F. S., 1989, Empirical calibration of geobarometers for the assemblage garnet-hornblende-plagioclase-quartz: American Mineralogist, v. 74, p. 77–84.

Kohn, M. J., and Spear, F. S., 1990, Two new geobarometers for garnet amphibolites with applications to eastern Vermont: American Mineralogist, v. 75, p. 89–96.

Krogh, T. E., 1973, A low-contamination method for hydrothermal decomposition of zircon and extraction of U and Pb for isotopic age determinations: Geochimica et Cosmochimica Acta, v. 37, p. 485–494.

Kruse, S., McNutt, M., Phipps-Morgan, J., Royden, L., and Wernicke, B., 1991, Lithospheric extension near Lake Mead, Nevada: A model for ductile flow in the lower crust: Journal of Geophysical Research, v. 96, p. 4435–4456.

Lachenbruch, A. H., and Sass, J. H., 1978, Models of an extending lithosphere and heat flow in the Basin and Range province, *in* Smith, R. B., and Eaton, G. P., eds., Cenozoic tectonics and regional geophysics of the Western Cordillera: Geological Society of America Memoir 152, p. 209–250.

Laird, J., and Albee, A. L., 1981, Pressure, temperature, and time in mafic schist: Their application to reconstruction of the polymetamorphic history of Vermont: American Journal of Science, v. 281, p. 127–175.

Leake, B. E., 1978, Nomenclature of amphiboles: American Mineralogist, v. 63, p. 1023–1052.

Lush, A. P., McGrew, A. J., Snoke, A. W., and Wright, J. E., 1988, Allochthonous Archean basement in the East Humboldt Range, Nevada: Geology, v. 16, p. 349–353.

MacCready, T., Snoke, A. W., Wright, J. E., and Howard, K. A., 1997, Mid-crustal flow during Tertiary extension in the Ruby Mountains core complex, Nevada: Geological Society of America Bulletin, v. 109, p. 1576–1594.

Mattinson, J. M. 1987, U-Pb ages of zircons: A basic examination of error propagation: Chemical Geology, Isotope Geoscience Section, v. 66, p. 151–162.

McGrew, A. J., 1992, Tectonic evolution of the northern East Humboldt Range, Elko County, Nevada [Ph.D. dissert]: Laramie, University of Wyoming, 191 p.

McGrew, A. J., and Casey, M., 1998, Quartzite fabric transition in a Cordilleran metamorphic core complex, *in* Snoke, A. W., Tullis, J. A., and Todd, V. R., eds., Fault-related rocks—A photographic atlas: Princeton, New Jersey, Princeton University Press, p. 484–489.

McGrew, A. J., and Snee, L. W., 1994, $^{40}Ar/^{39}Ar$ thermochronometric constraints on the tectonothermal evolution of the northern East Humboldt Range metamorphic core complex, Nevada: Tectonophysics, v. 238, p. 425–450.

McGrew, A. J., and Snoke, A. W., 1990, Styles of deep-seated flow in an expanding orogen: The record from the East Humboldt Range, Nevada: Geological Society of America Abstracts with Programs, v. 22, no. 3, p. 66.

Miller, D. M., Hillhouse, W. C., Zartman, R. E., and Lanphere, M. A., 1987, Geochronology of intrusive and metamorphic rocks in the Pilot Range, Utah and Nevada, and comparison with regional patterns: Geological Society of America Bulletin, v. 99, p. 866–879.

Mueller, K. J., and Snoke, A. W., 1993, Progressive overprinting of normal fault systems and their role in Tertiary exhumation of the East Humboldt–Wood Hills metamorphic complex, northeast Nevada: Tectonics, v. 12, p. 361–371.

Muncill, G. E., and Chamberlain, C. P., 1988, Crustal cooling rates inferred from homogenization of metamorphic garnets: Earth and Planetary Science Letters, v. 87, p. 590–596.

Peters, M. T., 1992, A petrologic and stable isotope study of the role of fluids in high-grade metamorphism: The East Humboldt Range, Nevada, USA [Ph.D. dissert.]: Chicago, University of Chicago, 279 p.

Peters, M. T., and Wickham, S. M., 1994, Petrology of upper amphibolite facies marbles from the East Humboldt Range, Nevada, USA: Evidence for high-temperature, retrograde, hydrous volatile fluxes at mid-crustal levels: Journal of Petrology, v. 35, p. 205–238.

Peters, M. T., and Wickham, S. M., 1995, On the causes of ^{18}O-depletion and $^{18}O/^{16}O$ homogenization during regional metamorphism: The East Humboldt Range core complex, Nevada: Contributions to Mineralogy and Petrology, v. 119, p. 68–82.

Peters, M. T., Wickham, S. M., and Miller, D. M., 1992, High $d^{13}C$ Late Proterozoic carbonates of the North American Cordillera: Geological Society of America Abstracts with Programs, v. 24, no. 7, p. 114.

Potter, C. J., Dubiel, R. F., Snee, L. W., and Good, S. C., 1995, Eocene extension of early Eocene lacustrine strata in a complexly deformed Sevier-Laramide hinterland, northwest Utah and northeast Nevada: Geology, v. 23, p. 181–184.

Powell, R., 1978, Equilibrium thermodynamics in petrology: An introduction: London, Harper & Row, 284 p.

Powell, R., and Holland, T. J. B., 1988, An internally consistent thermodynamic data set with uncertainties and correlations: 3. Applications to geobarometry, worked examples and a computer program: Journal of Metamorphic Geology, v. 6, p. 173–204.

Silverberg, D. S., 1990, Denudation rates and timing of diachronous Paleogene extension in south-central Idaho: Geological Society of America Abstracts with Programs, v. 22, no. 7, p. A330.

Snoke, A. W., and Lush, A. P., 1984, Polyphase Mesozoic-Cenozoic deformational history of the northern Ruby Mountains–East Humboldt Range, Nevada, *in* Linz, J., Jr., ed., Western geological excursions, Geological Society of America Annual Meeting: Reno, University of Nevada, v. 4, p. 232–260.

Snoke, A. W., and Miller, D. M., 1988, Metamorphic and tectonic history of the northeastern Great Basin, *in* Ernst, W. G., ed., Metamorphism and crustal evolution of the western United States (Rubey Volume VII): Englewood Cliffs, New Jersey, Prentice-Hall, p. 608–648.

Snoke, A. W., McKee, E. H., and Stern, T. W., 1979, Plutonic, metamorphic, and structural chronology in the northern Ruby Mountains, Nevada—A preliminary report: Geological Society of America Abstracts with Programs, v. 11, p. 520–521.

Snoke, A. W., McGrew, A. J., Valasek, P. A., and Smithson, S. B., 1990, A crustal cross-section for a terrain of superimposed shortening and extension: Ruby Mountains–East Humboldt Range metamorphic core complex, Nevada, *in* Salisbury, M. H., and Fountain, D. M., eds., Exposed cross-sections of the continental crust: Dordrecht, Holland, Kluwer Academic Publishers, p. 103–135.

Snoke, A. W., Wright, J. E., Hudec, M. R., and McGrew, A. J., 1992, Mesozoic magmatic-metamorphic-deformational history of the Ruby Mountains–East Humboldt Range, Nevada: Geological Society of America Abstracts with Programs, v. 24, no 6, p. 63.

Thorman, C. H., and Snee, L. W., 1988, Thermochronology of metamorphic rocks in the Wood Hills and Pequop Mountains, northeastern Nevada: Geological Society of America Abstracts with Programs, v. 20, p. A18.

Tracy, R. J., 1982, Compositional zoning and inclusions in metamorphic minerals, *in* Ferry, J. M., ed., Characterization of metamorphism through mineral equilibria: Mineralogical Society of America Reviews in Mineralogy, v. 10, p. 355–397.

Wernicke, B., 1990, The fluid crustal layer and its implications for continental dynamics, *in* Salisbury, M. H., and Fountain, D. M., eds., Exposed cross-sections of the continental crust: Dordrecht, Netherlands, Kluwer Academic Publishers, p. 509–544.

Wernicke, B., and Getty, S. R., 1997, Intracrustal subduction and gravity currents in the deep crust: Sm-Nd, Ar-Ar, and thermobarometric constraints from the Skagit Gneiss Complex, Washington: Geological Society of America Bulletin, v. 109, p. 1149–1166.

Wickham, S. M., and Peters, M. T., 1990, An oxygen isotope discontinuity in high-grade rocks of the East Humboldt Range, Nevada: Nature, v. 345, p. 150–153.

Wickham, S. M., and Peters, M. T., 1993, High $d^{13}C$ Neoproterozoic carbonate rocks in western North America: Geology, v. 21, p. 165–168.

Wickham, S. M., Taylor, H. P., Jr., Snoke, A. W., and O'Neil, J. R., 1991, An oxygen and hydrogen isotope study of high-grade metamorphism and anatexis in the Ruby Mountains–East Humboldt Range core complex, Nevada, *in* Taylor, H. P., Jr., O'Neil, J. R., and Kaplan, I. R., eds., Stable isotope geochemistry: A tribute to Samuel Epstein: Geochemical Society Special Publication 3, p. 373–390.

Wright, J. E., and Snoke, A. W., 1993, Tertiary magmatism and mylonitization in the Ruby–East Humboldt metamorphic core complex, northeastern Nevada: U-Pb geochronology and Sr, Nd, and Pb isotope geochemistry: Geological Society of America Bulletin, v. 105, p. 935–952.

MANUSCRIPT RECEIVED BY THE SOCIETY JUNE 25, 1997
REVISED MANUSCRIPT RECEIVED AUGUST 25, 1998
MANUSCRIPT ACCEPTED MARCH 4, 1999

Printed in U.S.A.